Molecular Therapy
Original Article

# microRNA-219 Reduces Viral Load and Pathologic Changes in Theiler's Virus-Induced Demyelinating Disease

Ana Lis Moyano,[1,5] Jeffrey Steplowski,[1] Haibo Wang,[2] Kyung-No Son,[3] Diana I. Rapolti,[1] Jeffrey Marshall,[1] Vince Elackattu,[1] Michael S. Marshall,[1] Amy K. Hebert,[1] Cory R. Reiter,[1] Viviana Ulloa,[1] Katarzyna C. Pituch,[1] Maria I. Givogri,[1] Q. Richard Lu,[2] Howard L. Lipton,[3] and Ernesto R. Bongarzone[1,4]

[1]Department of Anatomy and Cell Biology, College of Medicine, University of Illinois at Chicago, Chicago, IL 60612, USA; [2]Department of Pediatrics, Division of Experimental Hematology and Cancer Biology, Cincinnati Children's Hospital Medical Center, Cincinnati, OH 45229, USA; [3]Department of Microbiology and Immunology, College of Medicine, University of Illinois at Chicago, Chicago, IL 60612, USA; [4]Departamento de Química Biológica, Facultad de Farmacia y Bioquímica, Universidad de Buenos Aires, Argentina

**Analysis of microRNA (miR) expression in the central nervous system white matter of SJL mice infected with the BeAn strain of Theiler's murine encephalomyelitis virus (TMEV) revealed a significant reduction of miR-219, a critical regulator of myelin assembly and repair. Restoration of miR-219 expression by intranasal administration of a synthetic miR-219 mimic before disease onset ameliorates clinical disease, reduces neurogliosis, and partially recovers motor and sensorimotor function by negatively regulating proinflammatory cytokines and virus RNA replication. Moreover, RNA sequencing of host lesions showed that miR-219 significantly downregulated two genes essential for the biosynthetic cholesterol pathway, *Cyp51* (lanosterol 14-α-demethylase) and *Srebf1* (sterol regulatory element-binding protein-1), and reduced cholesterol biosynthesis in infected mice and rat CG-4 glial precursor cells in culture. The change in cholesterol biosynthesis had both anti-inflammatory and anti-viral effects. Because RNA viruses hijack endoplasmic reticulum double-layered membranes to provide a platform for RNA virus replication and are dependent on endogenous pools of cholesterol, miR-219 interference with cholesterol biosynthesis interfered virus RNA replication. These findings demonstrate that miR-219 inhibits TMEV-induced demyelinating disease through its anti-inflammatory and anti-viral properties.**

## INTRODUCTION

MicroRNAs (miRs) are small noncoding RNAs that regulate a myriad of biological processes by controlling gene expression.[1] Their dysregulation is associated with pathological conditions, suggesting the usefulness of synthetic miR mimics to restore or inhibit the levels of endogenous miRs.[2] CNS virus infections are of increasing interest as etiological agents causing neurological deficits in humans by directly targeting neuroglia[3] or as a bystander effect of virus-induced pathology.[4] Although miR-based therapies have been applied successfully to systemic virus infections and are under preclinical studies,[5,6] little is known about their usefulness in the context of CNS virus infections and CNS repair.

Theiler's murine encephalomyelitis virus (TMEV) produces chronic inflammation, together with a combination of oligodendrocyte (OL) death and immune-mediated demyelination, in susceptible mouse strains.[7] The low-neurovirulence TMEV BeAn strain provides a relevant experimental animal model for multiple sclerosis (MS), the most common demyelinating disease in adults.[8,9] Unlike the induction of demyelination by either chemical (lysolecithin and cuprizone) or immunological (experimental allergic encephalomyelitis [EAE]) means, TMEV-induced demyelination is the result of virus infection in its natural host. Demyelination in this setting requires persistence with a continuously replicating virus in an immunocompetent host to produce its immunopathology. Thus, TMEV infection in mice is an experimental model to assess candidate treatments for neurological dysfunction and myelin repair.

Gain- and loss-of-function studies have identified miR-219 as a key regulator of OL development, myelination, and remyelination.[10–12] miR-219 participates in OL maturation through repression of *Pdgfrα*, *Hes5*, *Sox6*, *Etv5*, and *Lingo1*, which inhibit OL differentiation,[11–13] and through cooperative interactions with miR-338 during remyelination.[13] The physiological significance of miR-219 in remyelination

Received 22 June 2017; accepted 11 January 2018;
https://doi.org/10.1016/j.ymthe.2018.01.008.

[5]Present address: Instituto Universitario de Ciencias Biomédicas de Córdoba (IUCBC), Córdoba, Argentina

**Correspondence:** Ana Lis Moyano, PhD, Department of Anatomy and Cell Biology, College of Medicine, University of Illinois at Chicago, 808 S. Wood St M/C 512, Chicago, IL 60612, USA.
**E-mail:** moyano@uic.edu
**Correspondence:** Ernesto R. Bongarzone, PhD, Department of Anatomy and Cell Biology, College of Medicine, University of Illinois at Chicago, 808 S. Wood St M/C 512, Chicago, IL 60612, USA.
**E-mail:** ebongarz@uic.edu

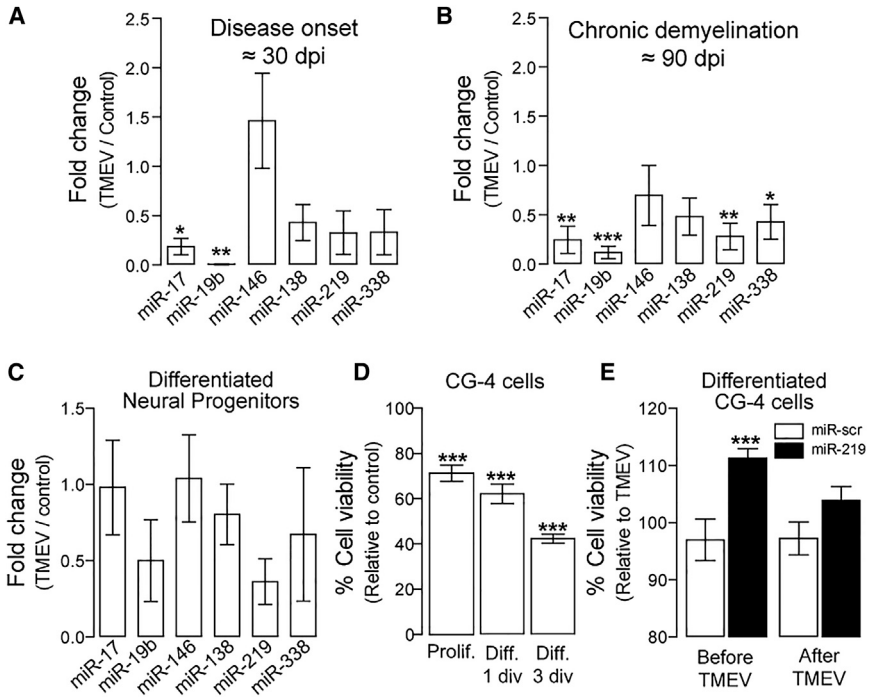


**Figure 1. Effects of BeAn Infection on OL-Related miRNAs**

(A and B) miRNA expression by qPCR of OL-related miRNAs, miR-17, miR-19b, miR-138, miR-219, miR-338, and astrocyte-related miR-146, in white matter of TMEV-infected mice at 30 days pi (A) and 90 days pi (B). One-way ANOVA followed by Dunnett's test: (A) $F$ (6, 30) = 5.472, *p < 0.05 and **p < 0.01 (n = 3 per group); and (B) $F$ (6, 32) = 4.346, *p < 0.05, **p < 0.01, and ***p < 0.001 (n = 3 per group). (C) miRNA expression by qPCR of OL-related miRNAs: miR-17, miR-19b, miR-138, miR-219, miR-338, and astrocyte-related miR-146 in neural stem cells differentiated for 2 days (n = 3). (D) Cell viability (WST-1 assay) of CG-4 cells at 24 hr after TMEV infection (10 MOI) under proliferating (PDGFAA) or differentiating conditions (1 div or 3 div). MOI, multiplicity of infection; div, days *in vitro*. (E) Cell viability in differentiated (3 div) CG-4 cells treated with miR-219 or scrambled miR (50 nM) before or after TMEV infection (10 MOI); one-way ANOVA followed by Dunnett's test, $F$ (2, 6) = 10.65, *p < 0.05 (n = 3 per group). Data are expressed as mean ± SEM.

is further supported by the finding of low miR-219 levels in non-remyelinating MS lesions.[14] These observations point to the promise of miR-219 treatment in restoring miR function and ameliorating myelin pathology. Previously, we successfully used miR-219 mimics to reduce chemical and inflammatory demyelination in lysolecithin and EAE models,[13] underscoring the potential utility of miR-219 for treatment of other types of demyelination.[15,16]

Here, we analyzed the therapeutic effects of miR-219 in a virus-induced demyelinating model. Following intranasal administration of miR-219 in TMEV-infected mice, we found significant reduction of clinical signs, virus persistence (virus genome copy numbers), neuroglia activation, proinflammatory cytokine levels, and demyelination. RNA sequencing of expressed host genes demonstrated that miR-219 potentiates transcriptional changes in cholesterol-related genes, leading to reduced levels of this lipid. Because virus replication relies on hijacking cholesterol biosynthesis and trafficking of host cell endogenous pools as well as remodeling intracellular membranes, i.e., the virus replication organelles or viroplasm,[17] treatment with miR-219 may interfere with virus RNA replication through downregulation of cholesterol synthesis. Our findings show that miR-219 administration lessens pathological changes by reducing the CNS virus loads and favoring myelin repair.[13]

## RESULTS

### BeAn Virus Infection Is Associated with Decreased miR-219 Levels

To determine whether BeAn virus infection modifies OL-related miRNA expression, white matter was isolated from the brains of mice at 30 (disease onset) and 90 (chronic demyelination) days post infection (pi) and analyzed by qPCR. Several OL-related miRNAs, including miR-17, miR-19b, miR-138, miR-219, and miR-338, were downregulated during early/acute (Figure 1A) and late/chronic (Figure 1B) stages of infection. Further experiments showed that after infection, miR-19b, miR-138, and miR-219 were substantially downregulated in differentiated neural progenitors isolated from the SJL mouse brain (Figure 1C). Of the downregulated miRs, miR-219 was of particular interest because it is downregulated in MS lesions and necessary for OL differentiation, myelination, and remyelination.[11–13] CG-4 cells, which were susceptible to BeAn infection (Figure 1D), were protected from infection when pre-treated with the miR-219 mimic (Figure 1E).

### *In Vivo* miR-219 Treatment Decreases Disease Severity

The therapeutic effects of miR-219 mimics were assessed in virus-infected mice treated weekly during 22 weeks via an intranasal route, a non-invasive drug administration method[18–20] (Figure 2A). To study biodistribution, Cy3-labeled miR mimics were first administered to naive SJL mice and analyzed by confocal microscopy. Cy3-labeled miR was distributed throughout the CNS, from the frontal cortex to spinal cord, with a gradient decreasing in a rostral-caudal direction (Figures S1A, S1B, and S1D), and taken up by multiple cell types, including astrocytes, microglia, neurons, and OLs (Figure S1C).

Cumulative disease scores of infected mice that received weekly doses of miR-219 for 22 weeks beginning before disease onset (Figure 2A) were significantly lower than those in mice treated with vehicle or scrambled miR (Figures 2B and 2C), indicating that treatment with miR-219 reduces disease severity in mice with demyelination.

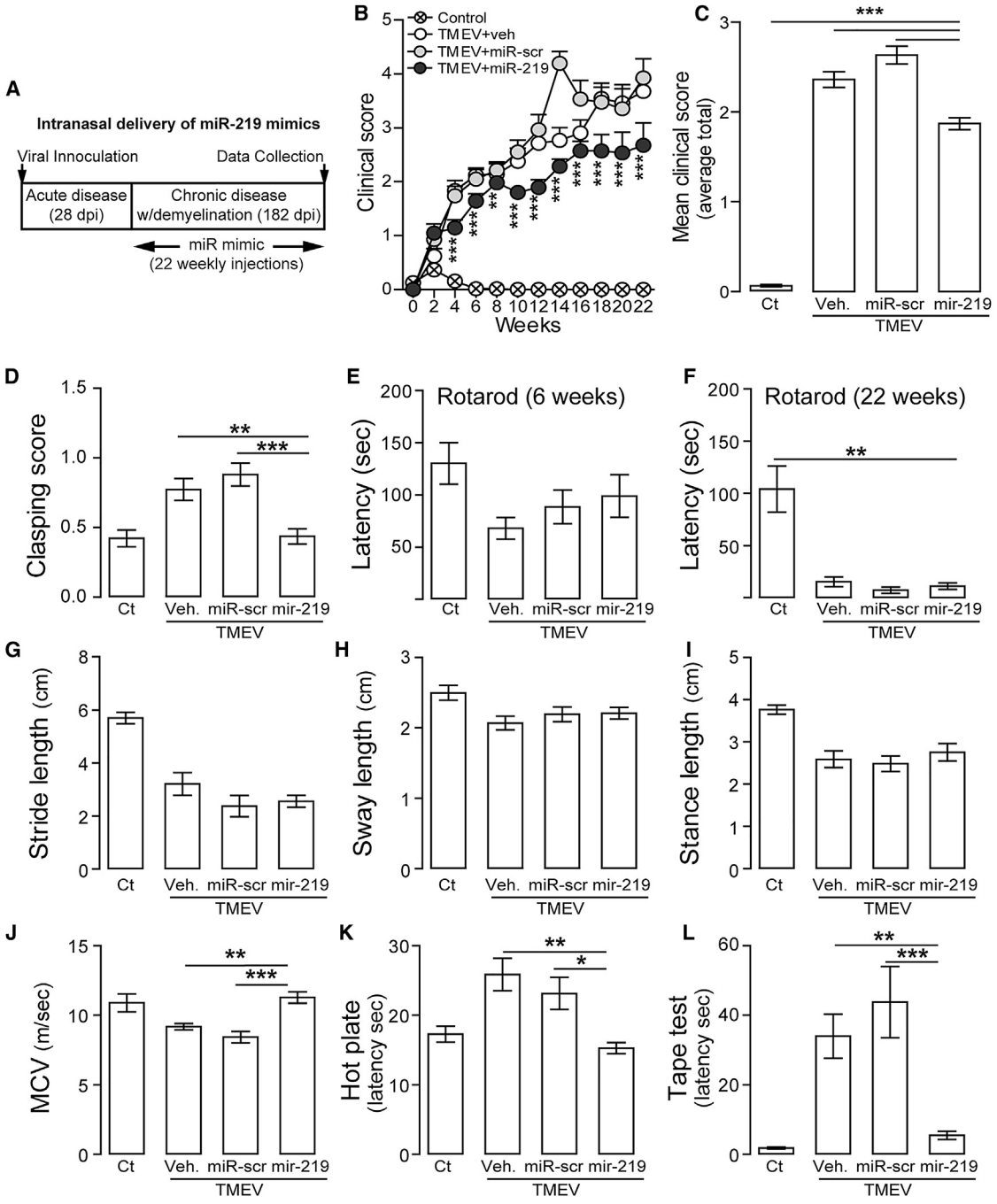


**Figure 2. miR-219 Decreases Disease Severity, Improves Sensorimotor Functions and Peripheral Nerve Conduction, but Not Balance or Motor Coordination**

(A) Experimental design of weekly supplementation therapy by intranasal delivery of synthetic miR-219 mimics. (B) Temporal progression of cumulative clinical score over treatment period in healthy animals (control) and mice with chronic demyelination treated with vehicle (TMEV+veh), scrambled miR (TMEV+miR-scr), or miR-219 (TMEV+miR-219). Two-way ANOVA followed by Bonferroni's test, $F$ (3, 1,033) = 9,016, $^{**}p < 0.01$ and $^{***}p < 0.001$ (n = 7 to 8 per group). (C) Cumulative clinical score over 22 weeks of treatment. One-way ANOVA followed by Tukey's test, $F$ (3, 1,078) = 281.3, $^{***}p < 0.001$ (n = 7 to 8 per group). Cumulative clinical score was calculated as the sum of the clinical score and body weight loss (see Materials and Methods). Data are expressed as mean ± SEM. (D) Clasping score: one-way ANOVA followed by Tukey's test, $F$ (3, 512) = 11.45, $^{**}p < 0.01$ and $^{***}p < 0.001$. (E and F) Balance and motor coordination analyzed by rotarod test: latency to fall (sec) in the experimental groups treated for 6 weeks (E) or 22 weeks (F). One-way ANOVA followed by Tukey's test in (F), $F$ (3, 80) = 16.43, $^{**}p < 0.01$. (G–I) Gait abnormalities assessed by footprint analysis: length (cm) of stride (G), sway (H), and stance (I) as an indication of motor coordination. (J) Motor nerve conduction velocity (MCV) (m/s) was determined on sciatic nerves. One-way

*(legend continued on next page)*

Assessment of motor and somatosensory functions using a battery of behavioral tests[21–23] in miR-219-treated mice revealed significant restoration of muscle and motor strength, as measured by reflexive hind limb clasping (Figure 2D), whereas coordination determined by the rotarod test (Figures 2E and 2F) and by the footprint test were not improved (Figures 2G–2I). Motor nerve function, as measured by motor conduction velocities in the sciatic nerve,[24] also recovered in miR-219-treated mice to that of healthy control nerves (Figure 2J). Somatosensory function, as determined using hot plate and tape removal tests, showed significant normalization toward control levels in miR-219-treated mice (Figures 2K and 2L). These results indicate that long-term miR-219 treatment improves CNS and peripheral nervous system (PNS) function and ameliorates many clinical signs of disease, although motor coordination did not recover. The nature of this difference might reflect a preferential effect of therapeutic miR-219 on sensory tracts (dorsal white matter) over that on motor tracts (ventral white matter) (Figure S1B).

### miR-219 Reduces Demyelination and Increases OL Numbers

To test whether improvement in clinical disease and neurological function correlates with pathological changes, sections of thoracic spinal cord, the site of greatest lesion severity, were plastic embedded, semithin sectioned, stained with toluidine blue, and analyzed for myelin structure (Figures 3A and 3B). The demyelinated axon density in dorsal and ventral white matter was significantly lower in infected mice treated with miR-219 compared to those treated with vehicle or scrambled miR. Dorsal white matter exhibited less demyelinated axons (~20%) than ventral white matter (~40%) (Figures 3C and 3D). In addition, myelin thickness (*g* ratio) in the dorsal and ventral white matter significantly normalized after miR-219 treatment (Figures 3E and 3F). In addition, Luxol fast blue staining (Figure 3G) demonstrated that miR-219 treatment reduced areas of demyelination by ~50% compared to infected mice treated with vehicle or scrambled miR (Figure 3H).

Confocal microscopy showed that miR-219 treatment improved expression of MBP (Figure 4A) without altering the number of neurons (NeuN+ cells) (Figures 4A and 4B) and significantly normalized the number of CC1+ OLs (Figures 4C and 4D). Expression analyses also revealed significantly greater levels of MBP proteins (Figures 4E and 4F), reduced numbers of OL precursors (OPCs) expressing *Pdgfrα* mRNA (Figure 4G and 4H), and PDGFRα protein levels (Figures 4I and 4J) in miR-219-treated mice than vehicle- or scrambled miR-treated mice. However, *Olig2* mRNA cell density was not affected in miR-219-treated mice (Figures 4K and 4L). Thus, weekly treatment with miR-219 reduced the relative amounts PDGFRα protein and *Pdgfrα* mRNA cells, which could in part be explained by fluctuations in their half-life and turnover,[25] with increased numbers of mature CC1+ oligodendrocytes in TMEV mice. Together, these results indicate that miR-219 treatment lessens disease severity and neurological dysfunction by reducing the amount of demyelination.

### miR-219 Reduces Microglia Activation, Astrogliosis, and Fibrinogen Leakage in Parallel to Reduction of Virus Copy Numbers

Inflammation is an important component of virus-induced demyelination.[26] To determine whether miR-219 treatment changes the inflammatory process, the status of resident microglia was assessed. The robust activation of microglia, which showed amoeboid morphology and increased cell density induced by infection, was mitigated by miR-219 compared to vehicle or scrambled miR (Figures S2A and 5D). Activation of astrocytes as measured by immunoblotting for Serpina3n[27] (Figures 5A and 5B) as well as the high expression of GFAP (Figures S2B, 5A, and 5C) were also significantly reduced in infected mice after treatment with miR-219. Leakage of fibrinogen into the CNS parenchyma[28] was also reduced (Figure S2C) in miR-219-treated mice, resulting in noticeably smaller areas of fibrinogen immunoreactivity.

Analysis of spinal cords to test whether pleiotropic effects of miR-219 in reducing the magnitude of virus-induced demyelination and gliosis involved changes in virus load by qPCR[29] revealed significantly fewer BeAn virus copies in infected mice with miR-219 than did mice treated with vehicle or scrambled miR (Figure 5E). Confocal microscopy of antibody-stained BeAn virus antigens revealed significant reduction of immunoreactivity in miR-219-treated mice compared to controls (Figures S2D and 5F), consistent with the effect of miR-219 on BeAn virus RNA replication and its persistence in the CNS.

### miR-219 Treatment Reduces Proinflammatory Cytokine Levels

To further examine changes in immune responses in infected mice, levels of proinflammatory cytokines were determined by multiplex ELISA in spinal cord protein extracts. Interleukin-10 (IL-10), IL-4, CXCL1, IL-1β, and tumor necrosis factor alpha (TNF-α) were significantly reduced in infected mice treated with miR-219 compared to vehicle and/or scrambled miR controls (Figures 6A–6C, 6G, and 6J), respectively, whereas levels of interferon-γ (IFN-γ), IL-2, and IL-6 did not change in treated mice (Figures 6D–6F). ELISA and western blot analysis of IL-1β signaling, which has been proposed to protect and promote demyelination during infection,[30] indicated significant recovery of IL-1β activation in miR-219-treated mice, returning levels to that of uninfected controls (Figures 6H and 6I). Levels of activated TNF-α (Figure 6K and 6L), important for apoptosis during infection,[31] were not normalized after treatment. Together, these results further support the beneficial role of miR-219 on gliosis and inflammation in the TMEV model.

ANOVA followed by Tukey's test, $F(3, 22) = 9.95$, $^{**}p < 0.01$ and $^{***}p < 0.001$. (K and L) Sensorimotor functions analyzed by hot plate (K) and tape test (L): latency (sec) to withdraw hindlimbs or forelimbs. One-way ANOVA followed by Tukey's test: (I) $F(3, 24) = 7.66$ and (J) $F(3, 20) = 15.19$, $^{*}p < 0.05$, $^{**}p < 0.01$, and $^{***}p < 0.001$. All tests included controls (Ct) and mice with chronic demyelination treated with vehicle (TMEV+veh), scrambled miR (TMEV+miR-scr), or miR-219 (TMEV+miR-219). Data are expressed as the mean ± SEM, n = 7 to 8 mice per group.

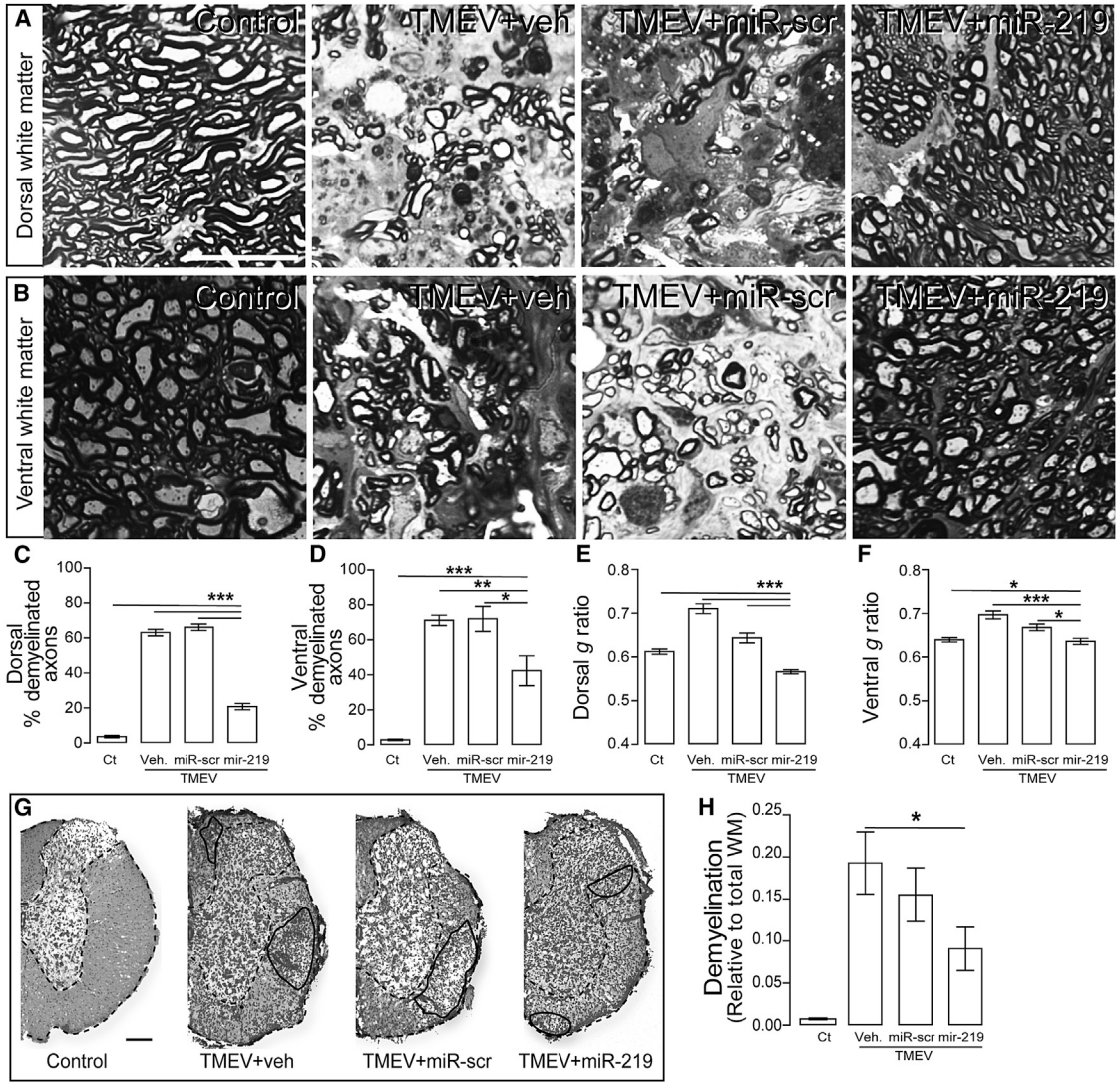


**Figure 3. Treatment with miR-219 Reduces TMEV-Mediated Demyelination**

(A and B) Representative micrographs of dorsal (A) and ventral (B) white matter in thoracic segments of the spinal cord; scale bar, 20 μm. (C–F) Demyelinated axons (% total axons) and myelin thickness (*g* ratio) were quantified in dorsal (C and E) and ventral (D and F) white matter from thoracic segments of the spinal cord; one-way ANOVA followed by Tukey's test: (C) $F(3, 27) = 157.1$, (D) $F(3, 29) = 44.5$, (E) $F(3, 850) = 81.4$, and (F) $F(3, 797) = 16.4$, *$p < 0.05$, **$p < 0.01$, and ***$p < 0.001$. (C–F) n = 3 per group. (G) Representative micrographs of Luxol fast blue and cresyl violet staining of thoracic segments of the spinal cord show demyelinated areas (solid line) relative to total white matter (WM) (dashed line); scale bar, 100 μm. (H) Quantification of demyelinated areas by Luxol fast blue and cresyl violet staining; one-way ANOVA followed by Tukey's test, $F(3, 32) = 10.45$, *$p < 0.05$ (n = 4 per group). Experimental groups: controls (Ct) and mice with chronic demyelination treated with vehicle (TMEV+veh), scrambled miR (TMEV+miR-scr), or miR-219 (TMEV+miR-219). Data are expressed as the mean ± SEM.

### miR-219 Potentiates Downregulation of Cholesterol-Related Genes

To compile a profile of transcriptional changes after miR-219 treatment, spinal cords were analyzed for expression of host genes by RNA sequencing. Although BeAn virus infection has consistently shown biological variability between experimental groups,[7] hierarchical clustering of gene expression pointed to two different groups of genes in infected mice (Figure S3A). GO functional enrichment analysis showed that for all groups, changes were mostly associated with immune biological processes (GEO: GSE107091; Table S1). These transcripts were upregulated in infected mice compared to healthy controls (see top segment of cluster 2 of the heatmap in Figure S3A), whereas a separate group of genes (cluster 1), primarily involved in cholesterol biosynthesis and synaptic vesicle trafficking, was substantially downregulated in miR-219-treated mice (Figure S3B). Comparison of genes from cluster 1 with a list of miR-219-predicted targets by Targetscan[32] showed that 4 of 388 predicted gene targets were present in cluster 1, including *Cyp51* (lanosterol 14-α demethylase) and *Insig1* (insulin-induced gene 1) (Figure S3C;

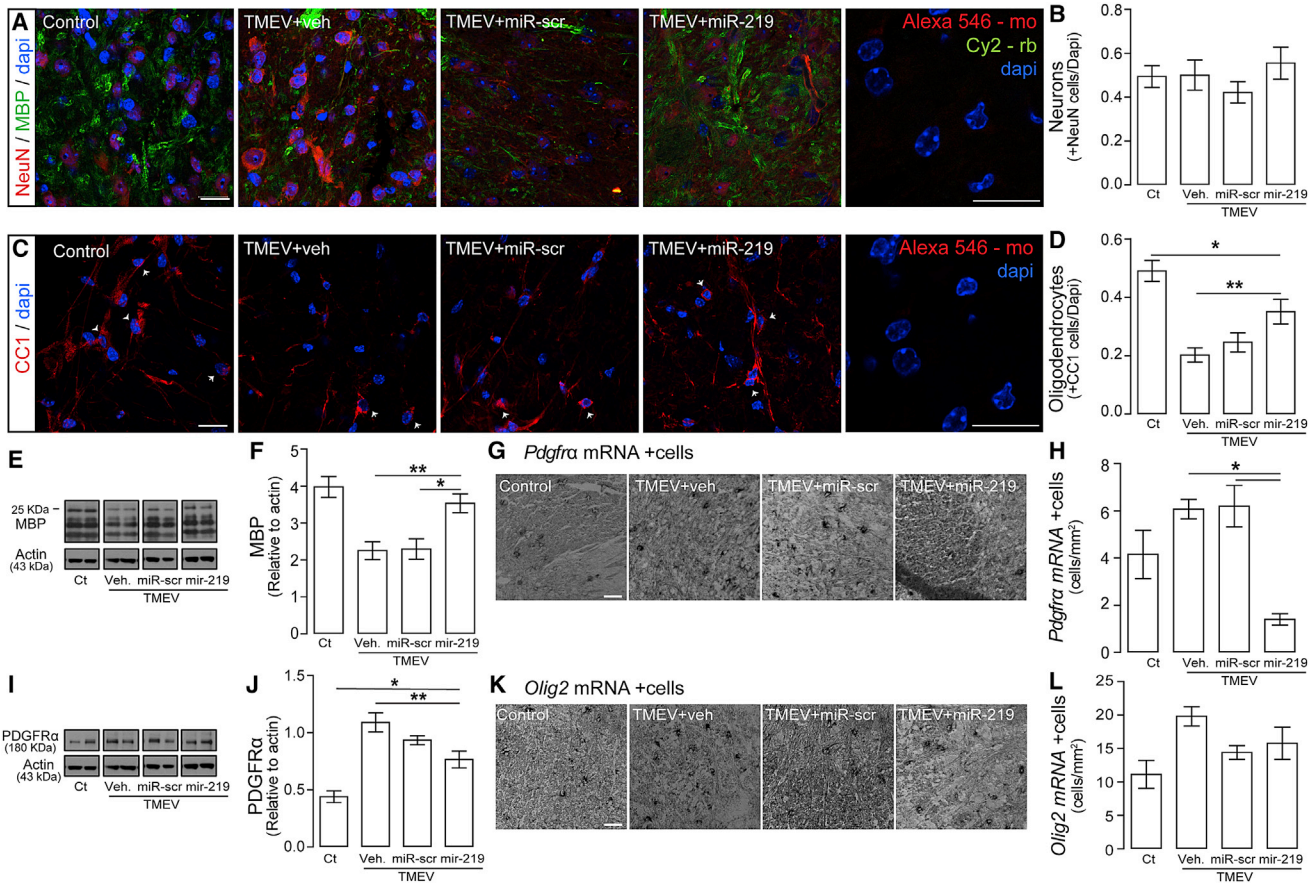


**Figure 4. Treatment with miR-219 Improves Myelination in TMEV-Infected Mice**

(A–D) Confocal microscopy quantitative analysis of MBP (myelin, green) and NeuN (neurons, red) (A and B) and of CC1 (OLs, red, arrowheads) (C and D) in thoracic spinal cord sections. Background staining controls of anti-mouse Alexa 546/anti-rabbit Cy5 and control anti-mouse Alexa 546 are shown. Nuclei were stained with DAPI (blue); scale bar, 20 μm. One-way ANOVA followed by Tukey's test, $F$ (3, 151) = 11.11, *p < 0.05 and **p < 0.01 (n = 4 per group). (E and F) Western blot analysis of MBP levels in protein extracts from the thoracic spinal cord (E); one-way ANOVA followed by Tukey's test (F), $F$ (3, 23) = 11.01, *p < 0.05 and **p < 0.01 (n = 7 to 8 per group). (G and H) *Pdgfrα*+ cells were counted after RNA *in situ* hybridization (G); scale bar, 40 μm; one-way ANOVA followed by Tukey's test (H), $F$ (3, 97) = 9.97, *p < 0.05 (n = 4 per group). (I and J) Western blot analysis of PDGFRα levels in protein extracts from the thoracic spinal cord (I); one-way ANOVA followed by Tukey's test (H), $F$ (3, 28) = 16.25, *p < 0.05 and **p < 0.01 (n = 7 to 8 per group). (K and L) *Olig2*+ cells were counted after RNA *in situ* hybridization (n = 4 per group); scale bar, 40 μm. Experimental groups: controls (Ct) and mice with chronic demyelination treated with vehicle (TMEV+veh), scrambled miR (TMEV+miR-scr), or miR-219 (TMEV+miR-219). Data are expressed as the mean ± SEM.

Table S1), which play essential roles in cholesterol biosynthesis.[33,34] qPCR analysis showed that *Cyp51* and *Hmgcs1* were both significantly reduced in mice treated with miR-219 relative to mice treated with vehicle or scrambled miR (Figures 7A and 7B). *Srebf1*, a master regulator of cholesterol biosynthesis,[35] was also significantly reduced by miR-219 (Figure 7C), whereas there were no significant differences for *Insig1*, *Hmgcr*, and *Srebf2* between the groups (Figures 7D–7F). Genes associated with cholesterol biosynthesis affected in infected mice treated with miR-219 (Figure S3) were not downregulated in normal non-infected OPCs or OLs after miR-219 treatment[13] (GEO: GSE80439) (Figures S4A and S4B). These findings indicate that in the context of BeAn virus infection, beneficial effects from miR-219 treatment were associated with transcriptional changes in genes related to cholesterol biosynthesis.

### miR-219 Decreases Cholesterol Levels

Inhibition of cholesterol biosynthesis has been shown to promote anti-viral immunity,[36] and, like other picornaviruses, BeAn virus replicates in remodeled intracellular membranes (viroplasm) by hijacking cholesterol trafficking and altering host lipid homeostasis.[17,37] Spectrofluorometric analysis to test whether downregulation of cholesterol-related genes was associated with changes in cholesterol levels revealed a significant reduction in cholesterol levels in the thoracic segment of the spinal cord of miR-219-treated mice compared to controls (Figure 8A). Similar results were observed with filipin staining of spinal cord sections by confocal microscopy (Figure 8B). Although changes in cholesterol after infection may be due in part to chronic demyelination, miR-219-treated mice showed less demyelination and significant reduction in cholesterol. To test

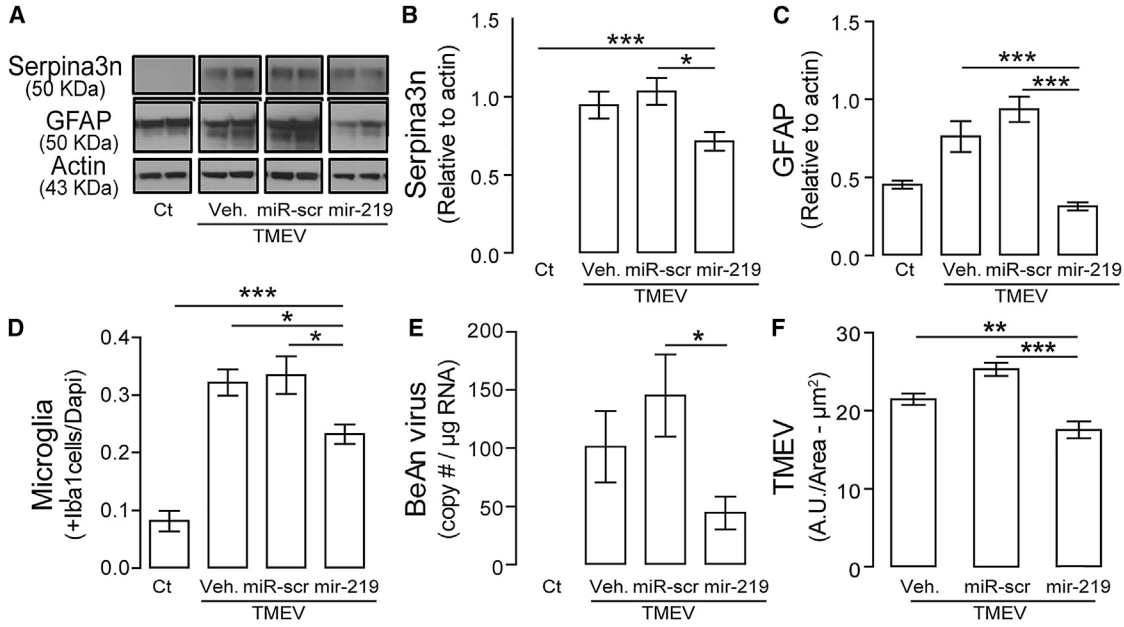


**Figure 5. miR-219 Reduces Astrogliosis, Microglia Activation, BeAn Copy Numbers, and Immunoreactivity**

(A) Astrogliosis was analyzed by western blotting of Serpina3n and GFAP in protein extracts from the thoracic spinal cord: (B) one-way ANOVA followed by Tukey's test, $F$ (3, 21) = 47.47, *p < 0.05 and ***p < 0.001 (n = 5–8 per group); and (C) one-way ANOVA followed by Tukey's test, $F$ (3, 21) = 17.03, ***p < 0.001 (n = 5–7 per group). (D) Microglia was quantified by confocal microscopy in thoracic segments of spinal cords; one-way ANOVA followed by Tukey's test, $F$ (3, 108) = 29.83, *p < 0.05 and ***p < 0.001 (n = 4 per group). (E) BeAn copy number by qPCR; one-way ANOVA followed by Tukey's test, $F$ (3, 26) = 7.62, *p < 0.05 (n = 7 to 8 per group). (F) BeAn capsid staining was quantified by confocal microscopy; one-way ANOVA followed by Tukey's test, $F$ (2, 72) = 19.15, **p < 0.01 and ***p < 0.001 (n = 4 per group). Experimental groups: control (Ct) and mice with chronic demyelination treated with vehicle (TMEV+veh), scrambled miR (TMEV+miR-scr), or miR-219 (TMEV+miR-219). Data are expressed as mean ± SEM.

whether miR-219 reduced cholesterol biosynthesis, differentiated CG-4 cells infected with BeAn virus (10 MOI), in the presence or absence of miR-219, were analyzed for cell viability and cholesterol levels. Cells treated with miR-219 showed a significant increase in viability compared to those treated with vehicle (Figures 8C and 8D), and depletion of cholesterol with methyl-β-cyclodextrin (MBCD) before infection showed similar results to those observed in miR-219-treated cells. Cholesterol levels in cells treated with miR-219 and MBCD were substantially reduced compared to those treated with vehicle or miR-scrambled, even at 24 hr pi (Figure 8E). Although primary OL and astrocyte cultures are less susceptible to TMEV infection *in vitro*,[38] cholesterol levels were substantially reduced in those cells treated with miR-219 before infection compared with scrambled miR-treated cells (Figure 8F). Thus, miR-219-induced changes in cholesterol biosynthesis may limit its availability for formation of membranes and active replication of TMEV, affecting virus RNA replication and alleviating viral effects on infected mice.

## DISCUSSION

Dysregulated miRs associated with different diseases can be corrected by rescue or inhibition using miR-based therapies. Here, we tested whether rescue of miR-219 in the BeAn virus infection is therapeutic. Indeed, treatment with miR-219 reduced virus-induced demyelination and clinical disease progression based on recovery of sensorimotor function, reduction of the CNS inflammatory response, and virus load. Transcriptional analysis showed that miR-219 downregulates cholesterol-related genes and lowers cholesterol levels in the CNS. Note that reduction of available cholesterol is a strategy to interfere with the life cycle of many RNA viruses.[17,39] However, we find that in the context of virus-induced demyelination, miR-219 shows additional physiological functions beyond its therapeutic effects in myelin repair.

During normal CNS myelination, miR-219 induces OL maturation by inhibiting neuronal differentiation from early undifferentiated neural precursors via repression of *NeuroD1* and *Zfp238* and by facilitating maturation of committed OPCs into mature OLs by repressing several key genes, including *Pdgfrα*, *Hes5*, *Sox6*, *Etv5*, and *Lingo1*.[11–13] Our recent gain- and loss-of-function studies identified an additional role for miR-219 in remyelination during lysolecithin- and EAE-induced demyelination.[13] In both chemical and immunologic-demyelinating paradigms, the pro-remyelinating properties of miR-219 were mediated by canonical repression of *Pdgfrα* expression in OPCs, driving OL maturation.[13] Similarly, lentiviral expression of miR-219 and transplantation of OPCs overexpressing miR-219 promoted remyelination and functional recovery after cuprizone-induced demyelination.[15,16] Here, we find an overall improvement in demyelination and

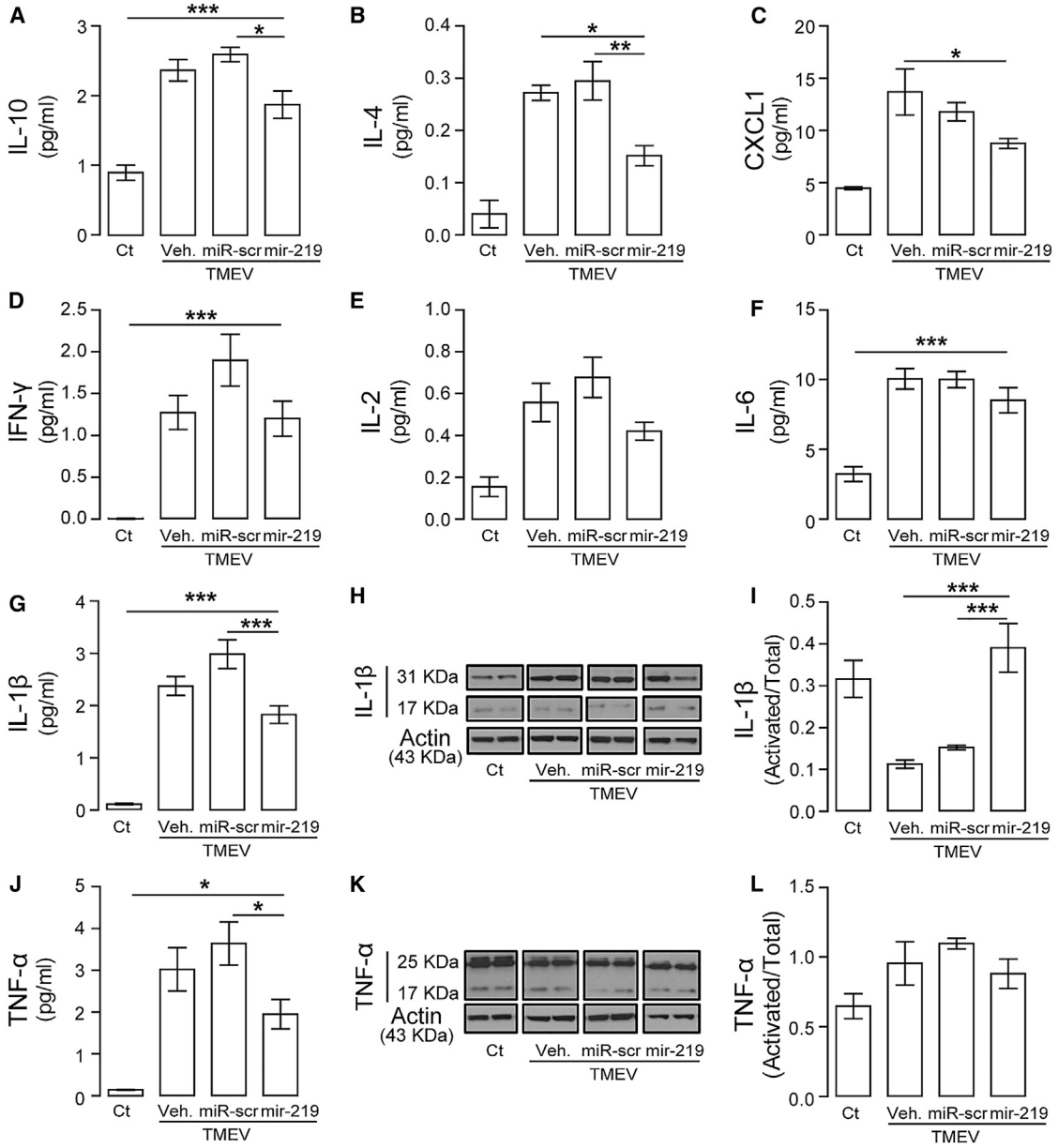


**Figure 6. miR-219 Reduces Proinflammatory Cytokines and Restores IL-1β Activation**

Quantitation of IL-10 (A), IL-4 (B), CXCL1 (C), IFN-γ (D), IL-2 (E), IL-6 (F), IL-1β (G), and TNF-α (J), respectively, in thoracic spinal cords analyzed by a multiplex ELISA: MSD proinflammatory panel; one-way ANOVA followed by Tukey's test: IL-10 $F$ (3, 17) = 32.62, IL-4 $F$ (3, 16) = 14.95, CXCL1 $F$ (3, 11) = 11.12, IFN-γ $F$ (3, 19) = 18.43, IL-2 $F$ (3, 22) = 8.16, IL-6 F (3, 19) = 26.23, IL-1β $F$ (3, 18) = 59.66, and TNF-α F (3, 18) = 19.41, *$p < 0.05$, **$p < 0.01$ and ***$p < 0.001$ (n = 5–7 per group). (H and I) Representative Western blot of active (17 KDa) and total (31 KDa) IL-1β expression (H) and band analysis of activated IL-1β normalized to the total protein (I). One-way ANOVA followed by Tukey's test $F$ (3, 21) = 13.94, ***$p < 0.001$ (n = 6–7 per group). (K and L) Representative Western blot of active (17 KDa) and total (25 KDa) TNF-α expression (K) and band analysis of activated TNF-α normalized to total protein levels (L). Experimental groups: control (Ct) and mice with chronic demyelination treated with vehicle (TMEV+veh), scrambled miR (TMEV+miR-scr) or miR-219 (TMEV+miR-219). Data are expressed as the mean ± SEM.

neurological function in infected mice through the anti-viral activity of miR-219. Potential miR-219-based therapies require extensive studies to improve specificity[40] and determine the therapeutic window for demyelinating diseases and virus-induced encephalomyelitis. Further studies are also needed to evaluate off-target gene silencing and potential side effects to avoid a deleterious outcome in the endogenous process of remyelination[41] and anti-viral immune response.

Picornaviruses such as TMEV replicate their RNA on host virus-remodeled membranes, termed viroplasm or replication organelles.[37,42]

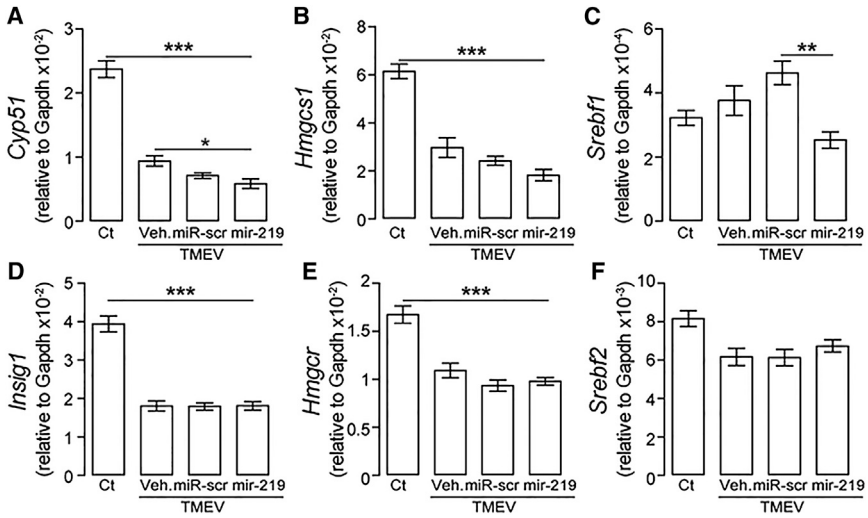


**Figure 7. miR-219 Potentiates Transcriptional Changes in Cholesterol-Related Genes**

(A–F) qPCR validation of genes from cluster 1 (see also Figures S3A and S3B) that are involved in cholesterol biosynthesis *Hmgcs1*: hydroxymethylglutaryl-CoA synthase (B), *Srebf1*: esterol regulatory element-binding protein 1 (C), *Hmgcr*: 3-hydroxy-3-methylglutaryl-coenzyme A reductase (E), and *Srebf2*: esterol regulatory element-binding protein 2 (F) and are also predicted targets of miR-219 (*Cyp51:* lanosterol 14-α demethylase, A, and *Insig1*: insulin-induced gene 1 protein, D); one-way ANOVA followed by Tukey's test: *Hmgcs1*, $F$ (3, 25) = 39.02; *Srebf1*, $F$ (3, 26) = 6.14; *Hmgcr*, $F$ (3, 27) = 24.91; *Srebf2*, $F$ (3, 29) = 5.45; *Cyp51*, $F$ (3, 23) = 77.44; and *Insig1*, $F$ (3, 27) = 59.09; *p < 0.05, **p < 0.01, and ***p < 0.001 (n = 5–8 per group). Experimental groups: control (Ct) and mice with chronic demyelination treated with vehicle (TMEV+veh), scrambled miR (TMEV+miR-scr), or miR-219 (TMEV+miR-219). Data are expressed as mean ± SEM.

Cholesterol is a key component of these organelles, and dysregulation of its biosynthesis or trafficking negatively impacts virus RNA replication.[17,39] Cholesterol-related genes, which were initially believed to play a role in inhibiting remyelination,[43] were found to be downregulated in infected mice, consistent with our RNA sequencing analysis showing that BeAn virus decreased expression of a cluster of genes involved in cholesterol biosynthesis. Unexpectedly, treatment with miR-219 potentiated these changes, with a further decrease in cholesterol levels in the spinal cord by miR-219-mediated downregulation of *Cyp51*, *Hmgcs1*, and *Srebf1*. By repressing cholesterol synthesis, miR-219 negatively regulated sustained virus RNA replication, leading to lower virus load, less demyelination, and amelioration of clinical disease. Thus, cholesterol-based therapies aimed to improve remyelination would not be as regenerative as expected,[44] despite the importance of cholesterol in myelin biogenesis.[45,46] Analysis of cells after *in vitro* depletion of cholesterol with MBCD confirmed that reduction of cholesterol leads to a protective effect similar to that observed with miR-219. Treatment with miR-219 more likely potentiated downregulation of genes involved in cholesterol biosynthesis in the context of TMEV infection because control experiments using non-infected OPCs and OLs treated with miR-219 did not show downregulation of these genes.

Changes in cholesterol biosynthesis affect anti-viral immunity by regulating the type I IFN response,[36] and chronic immune activation of IFN facilitates virus persistence.[47,48] We found that miR-219 treatment reduced the levels of IFN-γ, IL-4, IL-10, and CXCL1, while activating IL-1β, indicating highly selective effects on cytokine production. The mRNA levels of *Srebf1* were normalized after miR-219 treatment, and have been associated with IFN-mediated anti-viral responses by regulating IL-1β in inflammation.[49–51] Reduced inflammation likely reflects reduced virus RNA replication and reduced microglial activation and astrogliosis and a more competent blood-brain barrier. Clearly, miR-219 exerts pleiotropic effects on virus load and proinflammatory cytokines, ultimately leading to less demyelination and disease severity.

Together, our findings indicate that miR-219 induces beneficial effects in TMEV-infected mice, restoring neurological function and reducing virus-induced encephalomyelitis. These effects of miR-219 likely reflect its pro-remyelinating properties, the changes in the virus life cycle it induces by downregulating cholesterol-related genes, and the reduced availability of cholesterol to form replication organelles to sustain virus persistence. The specificity of these effects for miR-219 in BeAn virus infection is currently unclear but could be relevant to other viruses because several miRs play anti-viral roles in a wide spectrum of viral infections.[5,52–54] Overall, our study points to the promise of RNA-based therapies as an approach to reduce virus-induced demyelination, manipulation of the host response to virus infections, and impact virus persistence.

## MATERIALS AND METHODS

### Virus Culture

BHK-21 cells were grown in DMEM supplemented with 10% fetal bovine serum (FBS), 7.5% tryptose phosphate, 2 mM L-glutamine, 100 U/mL penicillin, and 100 μg/mL streptomycin at 37°C in a 5% $CO_2$ atmosphere. BeAn virus was amplified in BHK-21 cells and the titer of the virus stock was $2 \times 10^9$ plaque-forming unit (PFU)/mL. The origin and passage history of BeAn virus have been described.[55]

### TMEV Inoculation in Mice and Tissue Processing

All animal procedures were approved by the Institutional Animal Protection Committee at the University of Illinois at Chicago. SJL female mice (4–6 weeks old) were obtained from Harlan Laboratories. Mice were anesthetized and injected into the right cerebral hemisphere with 2 μL DMEM or DMEM containing $2 \times 10^6$ PFU/inoculum. Mice were allowed to recover and treated with miRNA mimics or vehicle at 28 days post-infection (dpi) (see below).

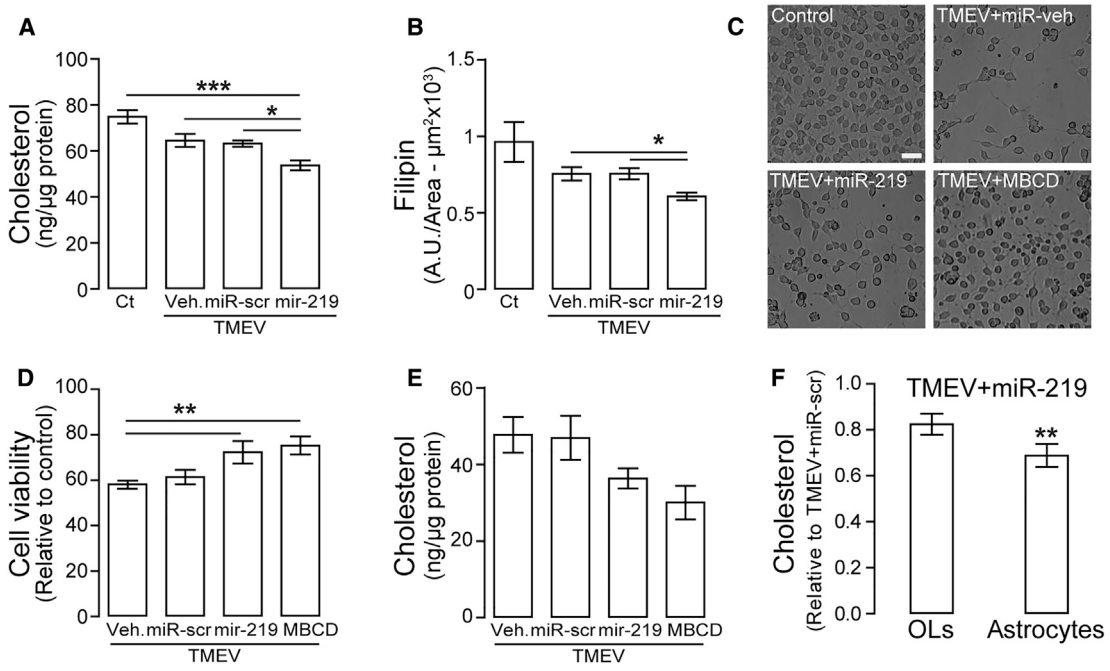


**Figure 8. miR-219 Reduces Cholesterol Levels *In Vivo* and *In Vitro***

(A) Cholesterol levels by the Amplex Red Cholesterol assay in thoracic spinal cords; one-way ANOVA followed by Tukey's test, $F(2, 21) = 10.44$, $^{*}p < 0.05$ and $^{***}p < 0.001$ (n = 6 to 7 per group). (B) Filipin (cholesterol) was measured after staining and analysis by confocal microscopy in thoracic spinal cord; one-way ANOVA followed by Tukey's test, $F(2, 66) = 4.05$, $^{*}p < 0.05$ (n = 4 per group). Experimental groups: control (Ct) and mice with chronic demyelination treated with vehicle (TMEV+veh), scrambled miR (TMEV+miR-scr), or miR-219 (TMEV+miR-219). (C and D) Micrographs of neuroglial CG-4 cells (C) and cell viability (WST-1 assay) (D), respectively, of CG-4 cells at 24 hr after TMEV infection (10 MOI) in differentiating conditions (3 div) treated with vehicle (TMEV+veh), scrambled miR (TMEV+miR-scr), miR-219 (TMEV+miR-219), or MBCD (1.5 mM) before infection; scale bar, 40 µm; one-way ANOVA followed by Tukey's test, $F(3, 13) = 9.08$, $^{**}p < 0.01$ (n = 3–6 per group). (E) Cholesterol levels measured by the Amplex Red Cholesterol assay in CG4 cells from (D). (F) Cholesterol levels by the Amplex Red Cholesterol assay of OL (n = 2) and astrocytes (n = 3) treated with miR-219 before TMEV infection. Student's t test, $t(4) = 5.55$, $^{**}p = 0.005$. Data are expressed as mean ± SEM.

For tissue collection, mice were anesthetized and perfused with phosphate buffer (0.2 M, pH 7.4). The right brain hemisphere and half of the cervical, thoracic, and lumbar spinal cords were post-fixed in 4% paraformaldehyde (PFA) overnight before processing for immunohistochemistry. The left-brain hemisphere and half of the cervical, thoracic, and lumbar spinal cords were immediately frozen for biochemical and transcriptional analyses. For immunohistochemistry, 30- to 40-µm sections were cut on a Leica SM2010 R sliding microtome and cryopreserved at −20°C in 30% glycerol and 30% ethylene glycol in 20 mM phosphate buffer until further use.

### Intranasal Administration of miRNA Mimics

miRNA mimics (Life Technologies) were mixed with transfection reagent i-Fect (Neuromics) at a ratio of 1:5 (w/v). Mice were treated with vehicle (i-Fect without mimics), scrambled miR (negative control #1, 4464059), or miR-219 (5′-UGAUUGUCCAAACGCAAU UCU-3′, 4464066 assay ID: MC10664) with i-Fect (2 µg miRNA). Intranasal delivery was completed over a 20-min period at a rate of 2 µL/min to alternating nostrils in slightly anesthetized animals. After 22 weeks (182 dpi) of supplementation with miRNA mimics, mice were euthanized and dissected for tissue processing.

### Clinical Score and Behavioral Tests

Assessment of clinical score and behavioral experiments were performed in standard animal room housing after 6 weeks (4-month-old mice) or 22 weeks (8-month-old mice) of treatment. Clinical scores: 1, mild waddling gait; 2, more severe waddling gait with extensor spams; and 3, lack of righting ability. Body weight loss: 0.5 (0.1–0.5 g); 1 (0.5–1 g); 1.5 (1–2 g), and 2 (>2 g). Cumulative clinical scores were calculated as the sum of the clinical and body weight loss scores. Sensorimotor functions were assessed at different time points of miRNA supplementation by the following behavioral tests. Clasping score: mice were held by their tails, observed for hindlimb position for 10 s, and scored as 0 (splayed out); 1 (retracted toward abdomen <5 s); 2 (retracted toward the abdomen >5 s); and 3 (entirely retracted and touching the abdomen >5 s). Hot plate test: mice were placed on a hot plate (52°C–55°C) enclosed by a compartment; latency for paw withdrawal was measured, with a cutoff time set to 10 s to avoid tissue damage. Tape test: a rectangular strip of tape was placed on the forepaws of mice and the time between contact of the mouse with the surface of the cage and either shaking its paws and/or directly bringing its paws to its mouth was measured. Rotarod test: after mice completed 3 days of training (3 sessions of 5 min each, accelerating from 4 to 40 rpm over 5 min) in an in-house

built apparatus, a test trial was performed after 6 or 22 weeks of miRNA supplementation. Footprint analysis: mice with forelimb and hindlimb paws painted with red and blue nontoxic paint, respectively, were placed at the start of a cardboard walkway (90-cm long, 6-cm wide, and 15-cm high) and expected to walk along a strip of standard white paper. Prints were analyzed by measurements of stride, sway, and stance between steps for a minimum of 4 steps. The results of each behavioral test were averaged within each experimental group.

#### Nerve Conduction Studies

Mice were anesthetized and the sciatic nerve was exposed. Stimulation was delivered via dual gold needle electrodes to the sciatic nerve and action potentials were recorded on an iWorx 228S Recorder, with a 5-lead electrocardiography (ECG)/electroencephalogram (EEG)/electromyography (EMG) cable within the gastrocnemius muscle.

#### Immunohistochemistry and Imaging

Tissue sections were blocked with 1% BSA, 10% donkey serum, 1% gelatin 0.3 M glycine, and 0.4% Triton X-100 in PBS for 1 hr at 25°C and incubated with the following primary antibodies for 72 hr at 4°C: PDGFRα 1:200 (Cell Signaling, 3164 and 3174); anti-Olig2 1:200 (Millipore, MABN50); CC1 1:50 (Millipore, OP80); MBP 1:1,000 (generous gift of Dr. Anthony Campagnoni, UCLA; rabbit polyclonal); NeuN 1:200 (Millipore, MAB377); GFAP 1:2,000 (Millipore, MAB3402); NG2 1:200 (Millipore, MAB5384); Iba1 1:1,000 (Wako, 019-19741), fibrinogen 1:200 (Agilent-Dako, A0080); and TMEV 1:2,000 (rabbit polyclonal). After washing 3 times in PBS, sections were incubated with the corresponding secondary antibody for 24 hr at 4°C: goat anti-mouse IgG (H+L); Alexa Fluor 546 1:1,000 (Life Technologies, A-11030); or Cy-2 IgG fraction monoclonal mouse anti-rabbit IgG (light chain-specific) 1:1,000 (Jackson ImmunoResearch, 211-222-171); and were covered with mounting media containing DAPI (Invitrogen, P36931). For cholesterol analysis, sections incubated with 50 μg/mL filipin (Polysciences, 08707) were incubated with To-pro-3 (Thermo Fisher Scientific, T3605). Fluorescence images were acquired with a Zeiss LSM 710 confocal microscope and quantified by ImageJ (NIH). RNA *in situ* hybridization was performed using digoxigenin-labeled *Pdgfrα* riboprobes as described.[12]

#### Luxol Fast Blue Myelin Staining

Tissue sections were stained with 0.1% Luxol fast blue solution (96% ethanol and 0.5% acetic acid) for 24 hr at 60°C, washed consecutively with 90% ethanol, $ddH_2O$, and 0.05% $Li_2CO_3$, and stained with 0.1% cresyl violet. Images were acquired with an automated Leica DM5500 B upright microscope, and areas of demyelination were quantitated using Image-J software for morphometric measurements.

#### G-ratio analysis

Tissue sections were fixed in electron microscopy fixative of 4% PFA and 2% glutaraldehyde. Tissue sections were post-fixed in 1% OsO4, dehydrated with ethanol, and embedded in Epon 812. Transverse semithin (1-μm) sections through the cervical cords were stained with Toludine blue. Images were acquired with an automated Leica DM5500 B upright microscope and quantified using ImageJ software. Myelin thickness (*g* ratio) was quantified as axon diameter/axon + myelin diameter (100 axons per anatomical region − dorsal and ventral white matter per animal; n = 3 mice per group).

#### Western Blotting

Tissue lysates were prepared and normalized to a protein content of 20 μg per sample by BCA assay (Pierce) and subjected to SDS polyacrylamide gel electrophoresis (4%–12%) using the XCell Sure-lock vertical electrophoresis system (Invitrogen). Gels were transferred to PVDF membranes, blocked with 5% milk in 0.1% Tris-buffered saline (TBS)-Tween 20 solution, and incubated for 24 hr at 4°C with the following primary antibodies: MBP 1:5,000 (rabbit polyclonal); actin 1:2,000 (Sigma, A2066); PDGFRα 1:1,000 (Cell Signaling, 3164 and 3174); anti-Olig2 1:500 (Millipore, MABN50); GFAP 1:2,000 (Millipore, MAB3402); Serpina3n 1:2,000 (R&D systems, AF4709); IL-1β (Abcam, ab9722); and TNF-α 1:500 (Cell Signaling, 3707). Incubation with secondary antibodies, anti-rabbit 1:1,000 (Cell Signaling, 7074), or anti-mouse 1:1,000 (Cell Signaling, 7076) was performed for 1 hr at 25°C, and membranes were developed using ECL (Pierce) and quantified using ImageJ software.

#### Amplex Red Cholesterol Assay

Cholesterol levels in cell or spinal cord homogenates (1–2 μL) were measured in 96-well plates using the fluorometric Amplex Red cholesterol assay kit according to the manufacturer's instructions (Invitrogen). Fluorimetric analysis was performed using a Beckman Coulter DTX 880 multimode detector (Molecular Devices).

#### Multiplex Cytokine ELISA

Thoracic spinal cord section homogenates in PBS (1:10 w/v) with mammalian protease inhibitor cocktail were sonicated and 1% Triton X-100 was added and incubated for 30 min at 4°C in an orbital shaker. After centrifugation at 12,000 × *g* for 20 min at 4°C, protein in each supernatant was quantified (BCA assay) and samples (150 μg protein) were analyzed using the V-PLEX Proinflammatory Panel 1 kit from Meso Scale Discovery (MSD) per the manufacturer's instructions in an MSD Sector Imager 2400.

#### RNA Extraction and qRT-PCR

Total RNA (including small RNAs) was purified from tissues or cell cultures using the miRVana miRNA isolation kit per the manufacturer's instructions (Life Technologies). RNA was transcribed to cDNA with the iScript cDNA Synthesis kit (Bio-Rad), and qRT-PCR was performed using the IQ5 real-time PCR detection system (Bio-Rad). Relative gene expression was normalized to *Gapdh*. qPCR primers were *Hmcgs1*: Forward: 5′-AACTGGTGCAGAAATCTCTAGC-3′, Reverse: 5′-GGTTG AATAGCTCAGAACTAGCC-3′, *Hmgcr*: Forward: 5′-AGCTTGCCC GAATTG-TATGTG-3′, Reverse: 5′-TCTGTTGTGAACCATGTGA CTTC-3′, *Cyp51*: Forward: 5′-GACAGGAGGCAACTTGCTTTC-3′, Reverse: 5′-GTGGACTTTTCGCTCCAGC-3′, *Insig1:* Forward: 5′-TC ACAGTGACTGAGCTTCAGCA-3′, Reverse: 5′-TCATCTTCA-TCA

CACCCAGGAC-3′, *Srebf2*: Forward 5′-GCAGCAACGGGACCAT TCT-3′, Reverse 5′-CCCCATGACTAAGTCCTTCAACT-3′, *Srebf1*: Forward: 5′-GATGTGCGAACTGG-ACACAG-3′, Reverse: 5′-CATA GGGGGCGTCAAACAG-3′, and *Gapdh:* Forward: 5′-AGGTCGGTG TGAACGGATTTG-3′, Reverse: 5′-TGTAGACCATGTAGTTGAGG TCA-3′.

To analyze miRNA expression, RNA samples were transcribed using the TaqMan MicroRNA Reverse Transcription kit (Applied Biosystems) and real-time PCR was performed on a ViiA 7 Real-Time PCR System (Applied Biosystems). Relative gene expression was normalized to U6. Applied Biosystems qPCR primers were: Assay ID: 002252 - Name: hsa-miR-338-3p, Assay ID: 000522 - Name: hsa-miR-219, Assay ID: 002284 - Name: hsa-miR-138, Assay ID: 001097 - Name: hsa-miR-146b, Assay ID: 000396 - Name: hsa-miR-19b, and Assay ID: 002308 - Name: hsa-miR-17.

### RNA Sequencing and Data Analysis

RNA isolated from spinal cords was analyzed by Next-Generation RNA Sequencing (Illumina). Raw reads were aligned to the reference genome using BWA MEM,[56] which efficiently maps reads with read-through into polyA tails and adaptor sequences, as is common with 3′ RNA-seq. Gene expression levels were quantified using FeatureCounts,[57] first as raw read counts suitable for differential expression analyses, and also normalized to reads-per-million for direct comparison between samples. Differential expression statistics (fold-change and p value) were computed using edgeR[58,59] on raw expression. Both multi-group tests between all experimental groups and pairwise tests between pairs of groups were performed, with p values adjusted for multiple testing using the false-discovery rate (FDR) correction of Benjamini and Hochberg[60] in all cases. Significant genes were identified based on an FDR threshold of 5% (0.05). GO analysis of genes was performed using GO Consortium (http://www.geneontology.org). RNA-seq data have been deposited in the NCBI Gene Expression Omnibus (GEO). GEO: GSE107091. OPC and OL gene expression levels were obtained at the NCBI GEO database,[61] GEO: GSE80439[13] (see also Table 1).

### Cell Culture and Transfection

CG-4 rat glial progenitor cells grown in DMEM/F12 (Gibco, 11330-032) supplemented with mitogens 10 ng/mL, PDGF-AA (Prepotech, 100-13A), and 5 ng/mL bFGF (Prepotech, 100-18B)[62] were allowed to differentiate for 1 or 3 days *in vitro* (1 days *in vitro* [div] or 3 div) in OL differentiation medium.[63] miRNA transfection was carried out with i-Fect using miRNA mimics at 50 nM. Neural stem cells were isolated from the telencephalon of 16-day SJL mouse embryos and maintained as neurospheres in suspension culture in medium containing 10 ng/mL bFGF and 20 ng/mL EGF (Prepotech, AF-100-15). Neurospheres were grown in NeuroCult basal medium (STEMCELL Technologies, 05700) under proliferative conditions (proliferation supplement, 05701) for 3–7 days, harvested, collected by centrifugation, suspended and mechanically dissociated, and maintained under proliferation or differentiation conditions (STEMCELL Technologies differentiation supplement, 05703). Mixed glial cultures were obtained as described,[64] with minor modifications.[63] Cortices were isolated from mouse pups (P2–P4) and glial cells were cultured in medium supplemented with 10% FBS (Atlanta, S11595H) for 14 to 15 days. After enrichment, astrocytes were grown in FBS-supplemented media and OL in specific medium[63] for 7–9 days. BHK-21 cells were grown in DMEM supplemented with 10% FBS, 7.5% tryptose phosphate (MP biomedicals, 091682149), and 2 mM L-glutamine (GIBCO, 25030149).

### *In Vitro* Virus Infection and Cholesterol Depletion

CG-4 cells were washed twice with Dulbecco's PBS and infected at an MOI of 1, 5, and 10 at 24°C for 45 min in serum-free medium, with rocking every 10 min to allow virus adsorption. Cells were maintained thereafter in fresh virus-free culture medium for 24 hr. For cholesterol depletion, cells were treated for 1 hr with 1.5 mM of methyl-β-cyclodextrin (Sigma, C4555) in DMEM/F12 supplemented with 25 mM HEPES before infection.

### Cell Viability Assay

WST-1 reagent (Roche) was added to the medium of monolayer cultures and incubated at 37°C in 5% $CO_2$ for 2–4 hr. Cell viability in samples was determined by absorbance at 420 nm (reference wavelength, 610 nm) against a background control (medium) using a microplate reader (Molecular Devices). Cell viability was calculated as the ratio of BeAn virus-infected to mock-infected cultures.

### Statistical Analyses

Each experimental condition was tested at least in duplicate, and animal studies utilized 7 or 8 mice per experimental group. Data were analyzed using one-way ANOVA followed by Dunnett's multiple comparison test or Tukey's post hoc test or two-way ANOVA followed by Bonferroni's post hoc test where appropriate. p values $< 0.05$ were considered significant. Data were analyzed using GraphPad Prism 6.00 (San Diego, CA, https://www.graphpad.com). Results are shown as the mean ± SEM, with horizontal bars representing significant differences between miR-219-treated infected mice compared to the rest of the experimental groups.

## SUPPLEMENTAL INFORMATION

Supplemental Information includes four figures and one table and can be found with this article online at https://doi.org/10.1016/j.ymthe.2018.01.008.

## AUTHOR CONTRIBUTIONS

A.L.M., Q.R.L., H.L.L., and E.R.B. designed the research. A.L.M., J.S., H.W., K.-N.S., D.I.R., J.M., V.E., M.S.M., A.K.H., C.R.R., V.U., K.C.P., and M.I.G. performed the research. A.L.M., H.L.L., and E.R.B analyzed the data. A.L.M., Q.R.L., H.L.L., and E.R.B. wrote the manuscript.

## CONFLICTS OF INTEREST

E.R.B. is a consultant for Lysosomal Therapeutics, Inc.

## ACKNOWLEDGMENTS

We thank Patricia Kallio, Zhiguo Liang, Emma Ward, Ludovic D'auria, and Danilo Ceschin for excellent technical assistance and Marina Hoffman for editorial assistance. E.R.B. was funded by NIH (R21NS087474) and the National Multiple Sclerosis Society (NMSS RG 4172). Q.R.L. was funded by NIH (R01NS072427) and the National Multiple Sclerosis Society (NMSS-RG-1507). H.L.L. was funded by NIH (NS065945) and Modestus Bauer Foundation grants.

## REFERENCES

1. Bartel, D.P. (2009). MicroRNAs: target recognition and regulatory functions. Cell *136*, 215–233.
2. Yin, H., Kanasty, R.L., Eltoukhy, A.A., Vegas, A.J., Dorkin, J.R., and Anderson, D.G. (2014). Non-viral vectors for gene-based therapy. Nat. Rev. Genet. *15*, 541–555.
3. Kondo, Y., Windrem, M.S., Zou, L., Chandler-Militello, D., Schanz, S.J., Auvergne, R.M., Betstadt, S.J., Harrington, A.R., Johnson, M., Kazarov, A., et al. (2014). Human glial chimeric mice reveal astrocytic dependence of JC virus infection. J. Clin. Invest. *124*, 5323–5336.
4. Koyuncu, O.O., Hogue, I.B., and Enquist, L.W. (2013). Virus infections in the nervous system. Cell Host Microbe *13*, 379–393.
5. Kapadia, S.B., Brideau-Andersen, A., and Chisari, F.V. (2003). Interference of hepatitis C virus RNA replication by short interfering RNAs. Proc. Natl. Acad. Sci. USA *100*, 2014–2018.
6. Rupaimoole, R., and Slack, F.J. (2017). MicroRNA therapeutics: towards a new era for the management of cancer and other diseases. Nat. Rev. Drug Discov. *16*, 203–222.
7. Lipton, H.L., Kumar, A.S.M., and Trottier, M. (2005). Theiler's virus persistence in the central nervous system of mice is associated with continuous viral replication and a difference in outcome of infection of infiltrating macrophages versus oligodendrocytes. Virus Res. *111*, 214–223.
8. Tsunoda, I., and Fujinami, R.S. (2010). Neuropathogenesis of Theiler's murine encephalomyelitis virus infection, an animal model for multiple sclerosis. J. Neuroimmune Pharmacol. *5*, 355–369.
9. Compston, A., and Coles, A. (2008). Multiple sclerosis. Lancet *372*, 1502–1517.
10. Shin, D., Shin, J.Y., McManus, M.T., Ptácek, L.J., and Fu, Y.H. (2009). Dicer ablation in oligodendrocytes provokes neuronal impairment in mice. Ann. Neurol. *66*, 843–857.
11. Dugas, J.C., Cuellar, T.L., Scholze, A., Ason, B., Ibrahim, A., Emery, B., Zamanian, J.L., Foo, L.C., McManus, M.T., and Barres, B.A. (2010). Dicer1 and miR-219 Are required for normal oligodendrocyte differentiation and myelination. Neuron *65*, 597–611.
12. Zhao, X., He, X., Han, X., Yu, Y., Ye, F., Chen, Y., Hoang, T., Xu, X., Mi, Q.S., Xin, M., et al. (2010). MicroRNA-mediated control of oligodendrocyte differentiation. Neuron *65*, 612–626.
13. Wang, H., Moyano, A.L., Ma, Z., Deng, Y., Lin, Y., Zhao, C., Zhang, L., Jiang, M., He, X., Ma, Z., et al. (2017). miR-219 cooperates with miR-338 in myelination and promotes myelin repair in the CNS. Dev. Cell *40*, 566–582.e5.
14. Junker, A., Krumbholz, M., Eisele, S., Mohan, H., Augstein, F., Bittner, R., Lassmann, H., Wekerle, H., Hohlfeld, R., and Meinl, E. (2009). MicroRNA profiling of multiple sclerosis lesions identifies modulators of the regulatory protein CD47. Brain *132*, 3342–3352.
15. Fan, H.-B., Chen, L.-X., Qu, X.-B., Ren, C.-L., Wu, X.-X., Dong, F.-X., Zhang, B.L., Gao, D.S., and Yao, R.Q. (2017). Transplanted miR-219-overexpressing oligodendrocyte precursor cells promoted remyelination and improved functional recovery in a chronic demyelinated model. Sci. Rep. *7*, 41407.
16. Liu, S., Ren, C., Qu, X., Wu, X., Dong, F., Chand, Y.K., Fan, H., Yao, R., and Geng, D. (2017). miR-219 attenuates demyelination in cuprizone-induced demyelinated mice by regulating monocarboxylate transporter 1. Eur. J. Neurosci. *45*, 249–259.
17. van der Schaar, H.M., Dorobantu, C.M., Albulescu, L., Strating, J.R.P.M., and van Kuppeveld, F.J.M. (2016). Fat(al) attraction: Picornaviruses usurp lipid transfer at membrane contact sites to create replication organelles. Trends Microbiol. *24*, 535–546.
18. Lee, S.-T., Chu, K., Jung, K.-H., Kim, J.H., Huh, J.-Y., Yoon, H., Park, D.K., Lim, J.Y., Kim, J.M., Jeon, D., et al. (2012). miR-206 regulates brain-derived neurotrophic factor in Alzheimer disease model. Ann. Neurol. *72*, 269–277.
19. Kim, I.-D., Shin, J.-H., Kim, S.-W., Choi, S., Ahn, J., Han, P.-L., Park, J.S., and Lee, J.K. (2012). Intranasal delivery of HMGB1 siRNA confers target gene knockdown and robust neuroprotection in the postischemic brain. Mol. Ther. *20*, 829–839.
20. Guardia Clausi, M., Paez, P.M., Campagnoni, A.T., Pasquini, L.A., and Pasquini, J.M. (2012). Intranasal administration of aTf protects and repairs the neonatal white matter after a cerebral hypoxic-ischemic event. Glia *60*, 1540–1554.
21. McGavern, D.B., Zoecklein, L., Drescher, K.M., and Rodriguez, M. (1999). Quantitative assessment of neurologic deficits in a chronic progressive murine model of CNS demyelination. Exp. Neurol. *158*, 171–181.
22. Lynch, J.L., Gallus, N.J., Ericson, M.E., and Beitz, A.J. (2008). Analysis of nociception, sex and peripheral nerve innervation in the TMEV animal model of multiple sclerosis. Pain *136*, 293–304.
23. Bouet, V., Boulouard, M., Toutain, J., Divoux, D., Bernaudin, M., Schumann-Bard, P., and Freret, T. (2009). The adhesive removal test: a sensitive method to assess sensorimotor deficits in mice. Nat. Protoc. *4*, 1560–1564.
24. Dolcetta, D., Amadio, S., Guerrini, U., Givogri, M.I., Perani, L., Galbiati, F., Sironi, L., Del Carro, U., Roncarolo, M.G., and Bongarzone, E. (2005). Myelin deterioration in Twitcher mice: motor evoked potentials and magnetic resonance imaging as *in vivo* monitoring tools. J. Neurosci. Res. *81*, 597–604.
25. Schwanhäusser, B., Busse, D., Li, N., Dittmar, G., Schuchhardt, J., Wolf, J., Chen, W., and Selbach, M. (2011). Global quantification of mammalian gene expression control. Nature *473*, 337–342.
26. Ercolini, A.M., and Miller, S.D. (2006). Mechanisms of immunopathology in murine models of central nervous system demyelinating disease. J. Immunol. *176*, 3293–3298.
27. Zamanian, J.L., Xu, L., Foo, L.C., Nouri, N., Zhou, L., Giffard, R.G., and Barres, B.A. (2012). Genomic analysis of reactive astrogliosis. J. Neurosci. *32*, 6391–6410.
28. Inoue, A., Koh, C.S., Yamazaki, M., Yanagisawa, N., Ishihara, Y., and Kim, B.S. (1997). Fibrin deposition in the central nervous system correlates with the degree of Theiler's murine encephalomyelitis virus-induced demyelinating disease. J. Neuroimmunol. *77*, 185–194.
29. Trottier, M., Schlitt, B.P., and Lipton, H.L. (2002). Enhanced detection of Theiler's virus RNA copy equivalents in the mouse central nervous system by real-time RT-PCR. J. Virol. Methods *103*, 89–99.
30. Kim, B.S., Jin, Y.-H., Meng, L., Hou, W., Kang, H.S., Park, H.S., and Koh, C.S. (2012). IL-1 signal affects both protection and pathogenesis of virus-induced chronic CNS demyelinating disease. J. Neuroinflammation *9*, 217.
31. Rubio, N., Martin-Clemente, B., and Lipton, H.L. (2003). High-neurovirulence GDVII virus induces apoptosis in murine astrocytes through tumor necrosis factor (TNF)-receptor and TNF-related apoptosis-inducing ligand. Virology *311*, 366–375.
32. Agarwal, V., Bell, G.W., Nam, J.W., and Bartel, D.P. (2015). Predicting effective microRNA target sites in mammalian mRNAs. eLife *4*, 1–38.
33. Lorbek, G., Lewinska, M., and Rozman, D. (2012). Cytochrome P450s in the synthesis of cholesterol and bile acids–from mouse models to human diseases. FEBS J. *279*, 1516–1533.
34. Kim, J.H., Jittiwat, J., Ong, W.Y., Farooqui, A.A., and Jenner, A.M. (2010). Changes in cholesterol biosynthetic and transport pathways after excitotoxicity. J. Neurochem. *112*, 34–41.
35. Shimano, H., Shimomura, I., Hammer, R.E., Herz, J., Goldstein, J.L., Brown, M.S., and Horton, J.D. (1997). Elevated levels of SREBP-2 and cholesterol synthesis in livers of mice homozygous for a targeted disruption of the SREBP-1 gene. J. Clin. Invest. *100*, 2115–2124.
36. York, A.G., Williams, K.J., Argus, J.P., Zhou, Q.D., Brar, G., Vergnes, L., Gray, E.E., Zhen, A., Wu, N.C., Yamada, D.H., et al. (2015). Limiting cholesterol biosynthetic flux spontaneously engages type I IFN signaling. Cell *163*, 1716–1729.
37. Ilnytska, O., Santiana, M., Hsu, N.Y., Du, W.L., Chen, Y.H., Viktorova, E.G., Belov, G., Brinker, A., Storch, J., Moore, C., et al. (2013). Enteroviruses harness the cellular

endocytic machinery to remodel the host cell cholesterol landscape for effective viral replication. Cell Host Microbe *14*, 281–293.

38. Qi, Y., and Dal Canto, M.C. (1996). Effect of Theiler's murine encephalomyelitis virus and cytokines on cultured oligodendrocytes and astrocytes. J. Neurosci. Res. *45*, 364–374.

39. Altan-Bonnet, N. (2017). Lipid tales of viral replication and transmission. Trends Cell Biol. *27*, 201–213.

40. de Fougerolles, A., Vornlocher, H.-P., Maraganore, J., and Lieberman, J. (2007). Interfering with disease: a progress report on siRNA-based therapeutics. Nat. Rev. Drug Discov. *6*, 443–453.

41. Plemel, J.R., Liu, W.Q., and Yong, V.W. (2017). Remyelination therapies: a new direction and challenge in multiple sclerosis. Nat. Rev. Drug Discov. *16*, 617–634.

42. Dorobantu, C.M., Albulescu, L., Harak, C., Feng, Q., van Kampen, M., Strating, J.R.P.M., Gorbalenya, A.E., Lohmann, V., van der Schaar, H.M., and van Kuppeveld, F.J. (2015). Modulation of the host lipid landscape to promote RNA virus replication: the picornavirus encephalomyocarditis virus converges on the pathway used by hepatitis C virus. PLoS Pathog. *11*, e1005185.

43. Ulrich, R., Kalkuhl, A., Deschl, U., and Baumgärtner, W. (2010). Machine learning approach identifies new pathways associated with demyelination in a viral model of multiple sclerosis. J. Cell. Mol. Med. *14*, 434–448.

44. Raddatz, B.B., Sun, W., Brogden, G., Sun, Y., Kammeyer, P., Kalkuhl, A., Colbatzky, F., Deschl, U., Naim, H.Y., Baumgärtner, W., et al. (2016). Central nervous system demyelination and remyelination is independent from systemic cholesterol level in Theiler's murine encephalomyelitis virus. Brain Pathol. *26*, 102–119.

45. Saher, G., Brügger, B., Lappe-Siefke, C., Möbius, W., Tozawa, R., Wehr, M.C., Wieland, F., Ishibashi, S., and Nave, K.A. (2005). High cholesterol level is essential for myelin membrane growth. Nat. Neurosci. *8*, 468–475.

46. Schmitt, S., Cantuti Castelvetri, L., and Simons, M. (2015). Metabolism and functions of lipids in myelin. Biochim. Biophys. Acta, Mol. Cell Biol. Lipids *1851*, 999–1005.

47. Teijaro, J.R., Ng, C., Lee, A.M., Sullivan, B.M., Sheehan, K.C.F., Welch, M., Schreiber, R.D., de la Torre, J.C., and Oldstone, M.B. (2013). Persistent LCMV infection is controlled by blockade of type I interferon signaling. Science *340*, 207–211.

48. Wilson, E.B., Yamada, D.H., Elsaesser, H., Herskovitz, J., Deng, J., Cheng, G., Aronow, B.J., Karp, C.L., and Brooks, D.G. (2013). Blockade of chronic type I interferon signaling to control persistent LCMV infection. Science *340*, 202–207.

49. Reboldi, A., Dang, E.V., McDonald, J.G., Liang, G., Russell, D.W., and Cyster, J.G. (2014). Inflammation. 25-Hydroxycholesterol suppresses interleukin-1-driven inflammation downstream of type I interferon. Science *345*, 679–684.

50. Oishi, Y., Spann, N.J., Link, V.M., Muse, E.D., Strid, T., Edillor, C., Kolar, M.J., Matsuzaka, T., Hayakawa, S., Tao, J., et al. (2017). SREBP1 contributes to resolution of pro-inflammatory TLR4 signaling by reprogramming fatty acid metabolism. Cell Metab. *25*, 412–427.

51. Cyster, J.G., Dang, E.V., Reboldi, A., and Yi, T. (2014). 25-Hydroxycholesterols in innate and adaptive immunity. Nat. Rev. Immunol. *14*, 731–743.

52. Robertson, K.A., Hsieh, W.Y., Forster, T., Blanc, M., Lu, H., Crick, P.J., Yutuc, E., Watterson, S., Martin, K., Griffiths, S.J., et al. (2016). An interferon regulated microRNA provides broad cell-Intrinsic antiviral immunity through multihit host-directed targeting of the sterol pathway. PLoS Biol. *14*, e1002364.

53. Huang, Y., Wang, W., and Ren, Q. (2016). Two host microRNAs influence WSSV replication via STAT gene regulation. Sci. Rep. *6*, 23643.

54. Ouyang, W., Wang, Y.S., Meng, K., Pan, Q.X., Wang, X.L., Xia, X.X., Zhu, Y.M., Bi, Z.W., Zhang, H.B., and Luo, K. (2017). gga-miR-2127 downregulates the translation of chicken p53 and attenuates chp53-mediated innate immune response against IBDV infection. Vet. Microbiol. *198*, 34–42.

55. Rozhon, E.J., Kratochvil, J.D., and Lipton, H.L. (1983). Analysis of genetic variation in Theiler's virus during persistent infection in the mouse central nervous system. Virology *128*, 16–32.

56. Li, H., and Durbin, R. (2010). Fast and accurate long-read alignment with Burrows-Wheeler transform. Bioinformatics *26*, 589–595.

57. Liao, Y., Smyth, G.K., and Shi, W. (2014). featureCounts: an efficient general purpose program for assigning sequence reads to genomic features. Bioinformatics *30*, 923–930.

58. McCarthy, D.J., Chen, Y., and Smyth, G.K. (2012). Differential expression analysis of multifactor RNA-Seq experiments with respect to biological variation. Nucleic Acids Res. *40*, 4288–4297.

59. Robinson, M.D., McCarthy, D.J., and Smyth, G.K. (2010). edgeR: a Bioconductor package for differential expression analysis of digital gene expression data. Bioinformatics *26*, 139–140.

60. Benjamini, Y., and Hochberg, Y. (1995). Controlling the false discovery rate: a practical and powerful approach to multiple testing. J. R. Stat. Soc. B *57*, 289–300.

61. Barrett, T., Wilhite, S.E., Ledoux, P., Evangelista, C., Kim, I.F., Tomashevsky, M., Marshall, K.A., Phillippy, K.H., Sherman, P.M., Holko, M., et al. (2013). NCBI GEO: archive for functional genomics data sets–update. Nucleic Acids Res. *41*, D991–D995.

62. Louis, J.C., Magal, E., Muir, D., Manthorpe, M., and Varon, S. (1992). CG-4, a new bipotential glial cell line from rat brain, is capable of differentiating *in vitro* into either mature oligodendrocytes or type-2 astrocytes. J. Neurosci. Res. *31*, 193–204.

63. O'Meara, R.W., Ryan, S.D., Colognato, H., and Kothary, R. (2011). Derivation of enriched oligodendrocyte cultures and oligodendrocyte/neuron myelinating co-cultures from post-natal murine tissues. J. Vis. Exp., Published online August 21, 2011. https://doi.org/10.3791/3324.

64. McCarthy, K.D., and de Vellis, J. (1980). Preparation of separate astroglial and oligodendroglial cell cultures from rat cerebral tissue. J. Cell Biol. *85*, 890–902.

**YMTHE, Volume *26***

## Supplemental Information

# microRNA-219 Reduces Viral Load and Pathologic Changes in Theiler's Virus-Induced Demyelinating Disease

**Ana Lis Moyano, Jeffrey Steplowski, Haibo Wang, Kyung-No Son, Diana I. Rapolti, Jeffrey Marshall, Vince Elackattu, Michael S. Marshall, Amy K. Hebert, Cory R. Reiter, Viviana Ulloa, Katarzyna C. Pituch, Maria I. Givogri, Q. Richard Lu, Howard L. Lipton, and Ernesto R. Bongarzone**

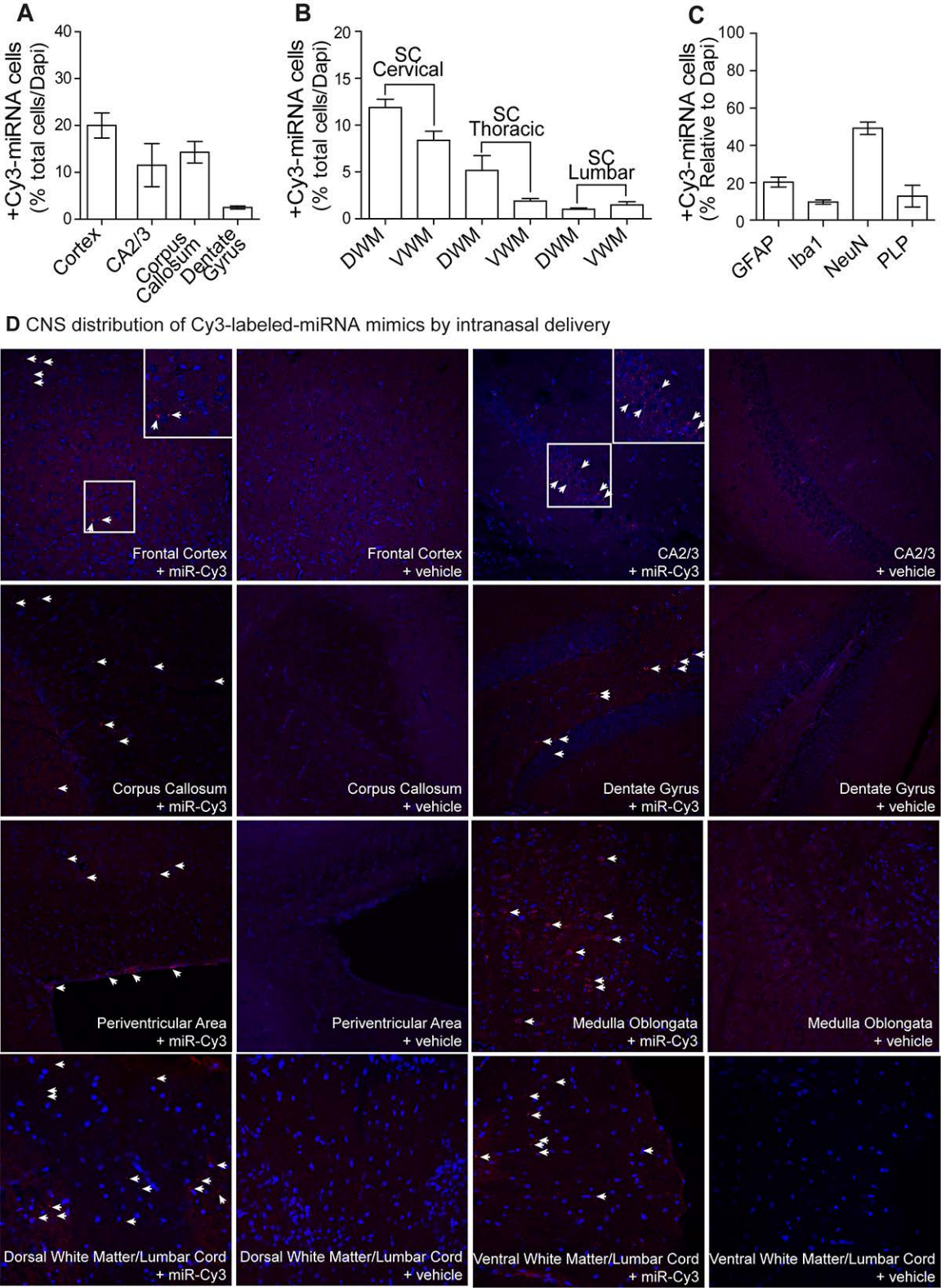
A
+Cy3-miRNA cells
(% total cells/Dapi)
40
30
20
10
0
Cortex
CA2/3
Corpus Callosum
Dentate Gyrus
B
+Cy3-miRNA cells
(% total cells/Dapi)
20
15
10
5
0
SC Cervical
SC Thoracic
SC Lumbar
DWM
VWM
DWM
VWM
DWM
VWM
C
+Cy3-miRNA cells
(% Relative to Dapi)
100
80
60
40
20
0
GFAP
Iba1
NeuN
PLP
D CNS distribution of Cy3-labeled-miRNA mimics by intranasal delivery
Frontal Cortex + miR-Cy3
Frontal Cortex + vehicle
CA2/3 + miR-Cy3
CA2/3 + vehicle
Corpus Callosum + miR-Cy3
Corpus Callosum + vehicle
Dentate Gyrus + miR-Cy3
Dentate Gyrus + vehicle
Periventricular Area + miR-Cy3
Periventricular Area + vehicle
Medulla Oblongata + miR-Cy3
Medulla Oblongata + vehicle
Dorsal White Matter/Lumbar Cord + miR-Cy3
Dorsal White Matter/Lumbar Cord + vehicle
Ventral White Matter/Lumbar Cord + miR-Cy3
Ventral White Matter/Lumbar Cord + vehicle

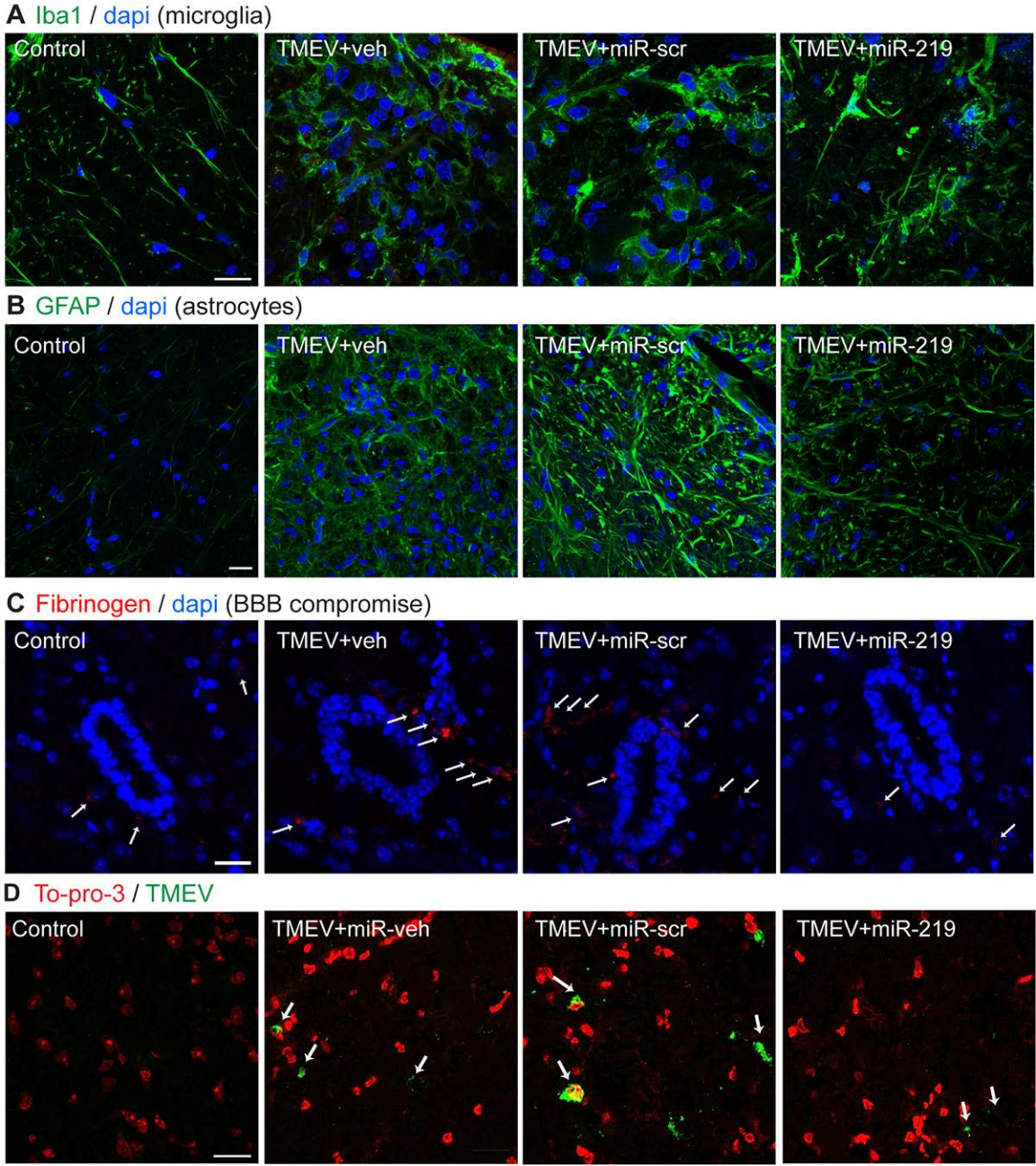
A Iba1 / dapi (microglia)
Control
TMEV+veh
TMEV+miR-scr
TMEV+miR-219
B GFAP / dapi (astrocytes)
Control
TMEV+veh
TMEV+miR-scr
TMEV+miR-219
C Fibrinogen / dapi (BBB compromise)
Control
TMEV+veh
TMEV+miR-scr
TMEV+miR-219
D To-pro-3 / TMEV
Control
TMEV+miR-veh
TMEV+miR-scr
TMEV+miR-219

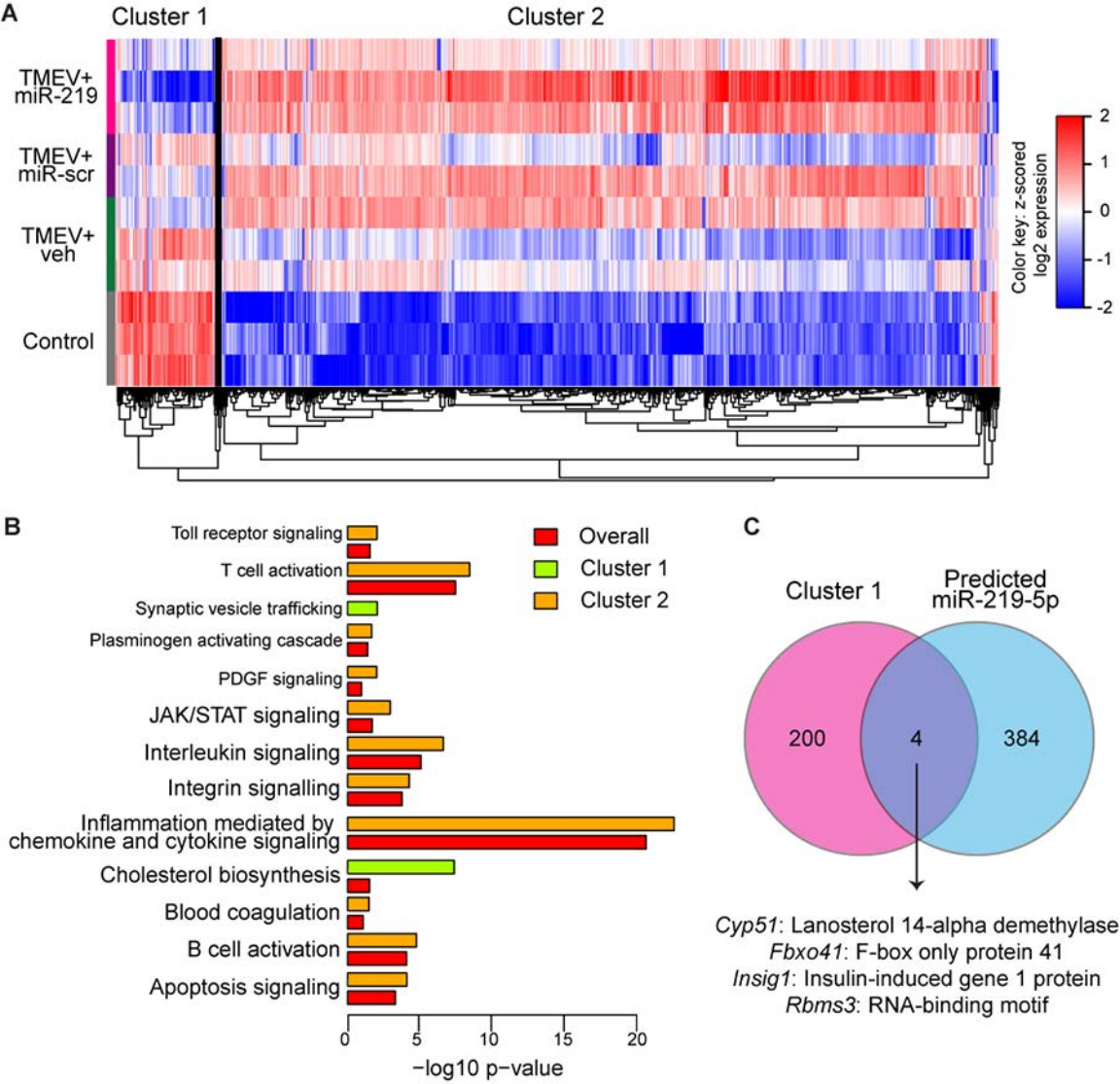
A
Cluster 1
Cluster 2
TMEV+ miR-219
TMEV+ miR-scr
TMEV+ veh
Control
Color key: z-scored log2 expression
2
1
0
-1
-2
B
Toll receptor signaling
T cell activation
Synaptic vesicle trafficking
Plasminogen activating cascade
PDGF signaling
JAK/STAT signaling
Interleukin signaling
Integrin signalling
Inflammation mediated by chemokine and cytokine signaling
Cholesterol biosynthesis
Blood coagulation
B cell activation
Apoptosis signaling
Overall
Cluster 1
Cluster 2
0
5
10
15
20
−log10 p−value
C
Cluster 1
Predicted miR-219-5p
200
4
384
Cyp51: Lanosterol 14-alpha demethylase
Fbxo41: F-box only protein 41
Insig1: Insulin-induced gene 1 protein
Rbms3: RNA-binding motif

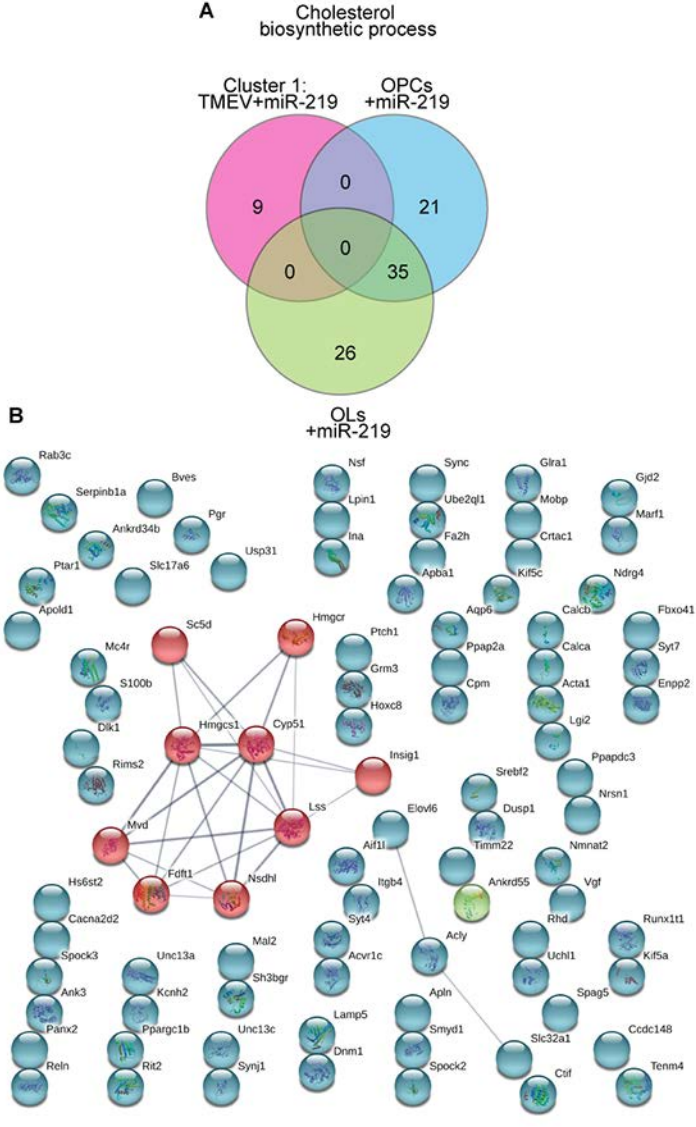
A
Cholesterol biosynthetic process
Cluster 1: TMEV+miR-219
OPCs +miR-219
OLs +miR-219
9
0
21
0
0
35
26
B
Rab3c
Serpinb1a
Bves
Pgr
Ankrd34b
Usp31
Ptar1
Slc17a6
Apold1
Nsf
Lpin1
Ina
Sync
Ube2ql1
Fa2h
Apba1
Glra1
Mobp
Crtac1
Kif5c
Gjd2
Marf1
Ndrg4
Aqp6
Calcb
Fbxo41
Syt7
Enpp2
Ppap2a
Cpm
Calca
Acta1
Lgi2
Ppapdc3
Nrsn1
Srebf2
Dusp1
Timm22
Ankrd55
Nmnat2
Vgf
Rhd
Runx1t1
Kif5a
Uchl1
Spag5
Ccdc148
Tenm4
Slc32a1
Csf
Apln
Smyd1
Spock2
Lamp5
Dnm1
Mal2
Sh3bgr
Unc13a
Kcnh2
Ppargc1b
Unc13c
Synj1
Rit2
Hs6st2
Cacna2d2
Spock3
Ank3
Panx2
Reln
Mc4r
S100b
Dlk1
Rims2
Sc5d
Hmgcr
Ptch1
Grm3
Hoxc8
Hmgcs1
Cyp51
Insig1
Lss
Mvd
Fdft1
Nsdhl
Elovl6
Arl1l
Itgb4
Syt4
Acly
Acvr1c

**Legends to Supplementary Figures**

**Figure S1. Biodistribution analysis of miR after intranasal delivery.** (**A-C**) The distribution of Cy3-labeled miR was examined throughout the neuroaxis by confocal microscopy. Cy3-miR were detected in all regions of the brain (**A**), the dorsal (DWM) and ventral (VWM) white matter spinal cord (SC) (**B**), and all cell types of the CNS: GFAP+ astrocytes, Iba+ microglia, NeuN+ neurons, and proteolipid PLP+ OLs (**C**). (n = 3 mice). (**D**) Confocal micrographs of Cy3 labeled-miR (arrows) distributed by intranasal delivery in different regions of the CNS. Nuclei stained with DAPI (blue), bar = 20 μm.

**Figure S2. miR-219 reduces gliosis, fibrinogen leakage, and TMEV immunoreactivity.** Representative confocal micrographs of Iba1+ microglia (**A**), and GFAP+ astrogliosis (**B**) in thoracic spinal cord sections. (**C**) Blood-brain barrier (BBB) permeability assessed by parenchymal fibrinogen staining (arrows) in thoracic spinal cord. (**D**) Representative confocal micrographs of BeAn capsid staining in thoracic spinal cord. Nuclei were stained with TO-PRO3 (red). Experimental groups: control (Ct) and mice with chronic demyelination treated with vehicle (TMEV+veh), scrambled miR (TMEV+miR-scr) or miR-219 (TMEV+miR-219). Nuclei stained with DAPI (blue), bar = 20 μm.

**Figure S3. miR-219 potentiates transcriptional changes in cholesterol-related genes.** (**A**) A heat-map of differentially expressed transcripts in in thoracic spinal cord of experimental groups. (**B**) GO analysis of the biological processes for gene clusters identified in (**A**). (**C**) Venn diagram showing overlap of genes from Cluster 1 and predicted targets for miR-219 by TargetScan. Experimental groups consist of healthy

mice (control) and mice with chronic demyelination treated with vehicle (TMEV+veh), scrambled miR (TMEV+miR-scr) or miR-219 (TMEV+miR-219).

**Figure S4: Venn diagram comparing Cluster 1 with downregulated genes in OPCs and OLs treated with miR-219.** (**A**) Genes related to cholesterol biosynthesis (GO analysis) from Cluster 1 in TMEV-infected animals treated with miR-219 compared with genes downregulated in OPCs and OLs treated with miR-219. (**B**) Gene network and enrichment analysis of Cluster 1 identified by STRING[1]. Functional interactions between cholesterol-related genes from Cluster 1 are the main connected component of the gene network analysis. These functional interactions were not present in OPCs and OLs treated with miR-219

**References:**

1. Szklarczyk, D, Morris, JH, Cook, H, Kuhn, M, Wyder, S, Simonovic, M, *et al*. (2017). The STRING database in 2017: quality-controlled protein–protein association networks, made broadly accessible. *Nucleic Acids Res*. **45**(D1):D362-D368